JPL Publication **00-3**

Chemical Kinetics and Photochemical Data for Use in Stratospheric Modeling

Supplement to Evaluation 12: Update of Key Reactions

Evaluation Number 13

NASA Panel for Data Evaluation:

S. P. Sander
R. R. Friedl
W. B. DeMore
Jet Propulsion Laboratory

A. R. Ravishankara
NOAA Environmental Research Laboratory

D. M. Golden
SRI International

C. E. Kolb
Aerodyne Research, Inc.

M. J. Kurylo
R. F. Hampson
R. E. Huie
National Institute of Standards and Technology

M. J. Molina
Massachusetts Institute of Technology

G. K. Moortgat
Max-Planck Institute for Chemistry

March 9, 2000

National Aeronautics and Space Administration

Jet Propulsion Laboratory
California Institute of Technology
Pasadena, California

The research described in this publication was carried out by the Jet Propulsion Laboratory, California Institute of Technology, under a contract with the National Aeronautics and Space Administration.

ABSTRACT

This is the thirteenth in a series of evaluated sets of rate constants and photochemical cross sections compiled by the NASA Panel for Data Evaluation.

The data are used primarily to model stratospheric processes, with particular emphasis on the ozone layer and its possible perturbation by anthropogenic and natural phenomena.

Copies of this evaluation are available in electronic form and may be printed from the following Internet URL:

http://jpldataeval.jpl.nasa.gov/

TABLE OF CONTENTS

TABLES

FIGURES

INTRODUCTION

This compilation of kinetic and photochemical data is an update to the 12th evaluation prepared by the NASA Panel for Data Evaluation. The Panel was established in 1977 by the NASA Upper Atmosphere Research Program Office for the purpose of providing a critical tabulation of the latest kinetic and photochemical data for use by modelers in computer simulations of stratospheric chemistry. Table I-1 lists this publication's editions:

Table I-1: Editions of this Publication

	Edition	Reference
1	NASA RP 1010, Chapter 1	(Hudson [1])
2	JPL Publication 79-27	(DeMore et al. [93])
3	NASA RP 1049, Chapter 1	(Hudson and Reed [2])
4	JPL Publication 81-3	(DeMore et al. [91])
5	JPL Publication 82-57	(DeMore et al. [89])
6	JPL Publication 83-62	(DeMore et al. [90])
7	JPL Publication 85-37	(DeMore et al. [84])
8	JPL Publication 87-41	(DeMore et al. [85])
9	JPL Publication 90-1	(DeMore et al. [86])
10	JPL Publication 92-20	(DeMore et al. [87])
11	JPL Publication 94-26	(DeMore et al. [88])
12	JPL Publication 97-4	(DeMore et al. [92])
13	JPL Publication 00-3	(Sander et al. [277])

Panel members and their major responsibilities are listed in Table I-2.

Table I-2: Panel Members and their Major Responsibilities for the Current Evaluation

Panel Members	Responsibility
S. P. Sander, Chairman M. J. Kurylo	Halogen chemistry
W. B. DeMore R. R. Friedl R. F. Hampson	HO_x chemistry, NO_x chemistry
D. M. Golden	Three-body reactions, equilibrium constants
R. E. Huie	Aqueous chemistry, thermodynamics
C. E. Kolb	Heterogeneous chemistry
A. R. Ravishankara	$O(^1D)$ chemistry Photochemical data
M. J. Molina G. K. Moortgat	Photochemical data

As shown above, each Panel member concentrates his efforts on a given area or type of data. Nevertheless, the Panel's final recommendations represent a consensus of the entire Panel. Each member reviews the basis for all recommendations, and is cognizant of the final decision in every case.

Communications regarding particular reactions may be addressed to the appropriate panel member:

S. P. Sander
R. R. Friedl
Jet Propulsion Laboratory
M/S 183-901
4800 Oak Grove Drive
Pasadena, CA 91109
ssander@jpl.nasa.gov
rfriedl@jpl.nasa.gov

D. M. Golden
PS-031
SRI International
333 Ravenswood Ave.
Menlo Park, CA 94025
golden@sri.com

R. E. Huie
M. J. Kurylo
National Institute of Standards and Technology
Physical and Chemical Properties Division
Gaithersburg, MD 20899
robert.huie@nist.gov
michael.kurylo@nist.gov

A. R. Ravishankara
NOAA-ERL, R/E/AL2
325 Broadway
Boulder, CO 80303
ravi@al.noaa.gov

C. E. Kolb
Aerodyne Research Inc.
45 Manning Rd.
Billerica, MA 01821
kolb@aerodyne.com

M. J. Molina
Department of Earth, Atmospheric, and Planetary Sciences
and Department of Chemistry
Massachusetts Institute of Technology
Cambridge, MA 02139
mmolina@mit.edu

G. K. Moortgat
Max-Planck-Institut für Chemie
Atmospheric Chemistry Division
Postfach 3060
55020 Mainz
Germany
moo@mpch-mainz.mpg.de

Basis of the Recommendations

The recommended rate data and cross sections are based on laboratory measurements. In order to provide recommendations that are as up-to-date as possible, preprints and written private communications are accepted, but only when it is expected that they will appear as published journal articles.

Under no circumstances are rate constants adjusted to fit observations of atmospheric concentrations. The Panel considers the question of consistency of data with expectations based on the theory of reaction kinetics, and when a discrepancy appears to exist this fact is pointed out in the accompanying note.

The major use of theoretical extrapolation of data is in connection with three-body reactions, in which the required pressure or temperature dependence is sometimes unavailable from laboratory measurements, and can be estimated by use of appropriate theoretical treatment. In the case of important rate constants for which no experimental data are available, the panel may provide estimates of rate constant parameters based on analogy to similar reactions for which data are available.

Scope of the Evaluation

In the past, the NASA Panel on Data Evaluation reviewed the entire set of reactions presented in the previous compilations, updating the recommendations and increasing the scope of the review in response to changes in the published literature [2,84-93,155].

For the current release, the Panel has focused on a selected subset of the kinetic and photochemical parameters presented in the JPL 97-4 evaluation [92]. The most important criterion which guided the scope of the present evaluation was an analysis of the sensitivities and uncertainties of reactions with respect to ozone depletion.

Guidance in this selection was obtained from several recent sensitivity analysis studies including those of Dubey et al. [102], Thompson and Stewart [316] and Chen et al. [59]. The reaction lists from these studies were used to identify those processes which play a particularly important role in ozone depletion calculations. Reactions were selected for inclusion (somewhat subjectively) if there were significant uncertainties in the laboratory data or if significant time had elapsed since the last evaluation.

Another important criterion was interpretating atmospheric field measurements. For example, the OH + NO_2 reaction has a significant effect on the ratio of NO_x to NO_y, which is measured by high precision aircraft instruments. On this basis, this reaction and several others were included in this update.

Because of the significant impact of heterogeneous reactions in the polar and mid-latitude lower stratosphere and rapid progress in laboratory investigations of these processes, several heterogeneous reactions were included in the present evaluation.

We currently lack guidance from multi-dimensional model sensitivity analyses as to which heterogeneous processes contribute the largest degrees of uncertainty to current stratospheric chemistry models. However, available box model calculations [102] indicate that uncertainties in heterogeneous reactions can lead to significant uncertainties in calculated ozone levels.

The six reactions identified as key heterogeneous processes most often included in current stratospheric photochemical models are listed below:

$$N_2O_5 + H_2O \rightarrow 2\ HNO_3$$
$$ClONO_2 + H_2O \rightarrow HOCl + HNO_3$$
$$ClONO_2 + HCl \rightarrow Cl_2 + HNO_3$$
$$HOCl + HCl \rightarrow Cl_2 + H_2O$$
$$BrONO_2 + H_2O \rightarrow HOBr + HNO_3$$
$$HOBr + HCl \rightarrow BrCl + H_2O$$

While each of these six reactions occurs to a greater or lesser extent on the full range of stratospheric aerosol surfaces, we have restricted this review to the three most frequently studied, and/or believed to be the most likely present in the stratosphere:

- Water ice,
- Nitric acid trihydrate, and
- Liquid sulfuric acid/water mixtures (typically ~40 to 80 wt.% H_2SO_4).

This selection of aerosol surface compositions covers those found in most current stratospheric models.

Format of the Evaluation

Changes or additions to the tables of data are indicated by shading. A new entry is completely shaded, whereas a changed entry is shaded only where it has changed. In some cases only the note has been changed, in which case the corresponding note number in the table is shaded. In the Photochemistry section, changed notes are indicated by shading of the note heading.

Computer Access

To ensure universal availability, this document is available online as a file in Adobe PDF (Portable Data File), Microsoft Word, and Postscript format. Files may be downloaded from http://jpldataeval.jpl.nasa.gov/. This document is not available in printed form from JPL.

Individuals who wish to receive notice when the web page is revised should submit email addresses in the appropriate reply box on the web page.

For more information, query Stanley Sander (Stanley.Sander@jpl.nasa.gov).

Data Formats

In Table 1 (Rate Constants for Second Order Reactions) the reactions are grouped into the classes $O(^1D)$, HOx, NOx, Hydrocarbon Reactions, ClOx and BrOx. The data in Table 2 (Rate Constants for Association Reactions) are presented in the same order as the bimolecular reactions. The presentation of photochemical cross section data follows the same sequence.

Units

The rate constants are given in units of concentration expressed as molecules per cubic centimeter and time in seconds. Thus, for first-, second-, and third-order reactions the units of k are s^{-1}, cm^3 $molecule^{-1}$ s^{-1}, and cm^6 $molecule^{-2}$ s^{-1}, respectively. Cross sections are expressed as cm^2 $molecule^{-1}$, base e.

BIMOLECULAR REACTIONS

Some of the reactions in Table 1 are actually more complex than simple two-body reactions. To explain the pressure and temperature dependences occasionally seen in reactions of this type, it is necessary to consider the bimolecular class of reactions in terms of two subcategories, direct (concerted) and indirect (nonconcerted) reactions.

A direct or concerted bimolecular reaction is one in which the reactants A and B proceed to products C and D without the intermediate formation of an AB adduct that has appreciable bonding, i.e., there is no bound intermediate; only the transition state $(AB)^{\neq}$ lies between reactants and products.

$$A + B \rightarrow (AB)^{\neq} \rightarrow C + D$$

The reaction of OH with CH_4 forming $H_2O + CH_3$ is an example of a reaction of this class.

Very useful correlations between the expected structure of the transition state $[AB]^{\neq}$ and the A-Factor of the reaction rate constant can be made, especially in reactions that are constrained to follow a well-defined approach of the two reactants in order to minimize energy requirements in the making and breaking of bonds. The rate constants for these reactions are well represented by the Arrhenius expression $k = A \exp(-E/RT)$ in the 200-300 K temperature range. These rate constants are not pressure dependent.

The indirect or nonconcerted class of bimolecular reactions is characterized by a more complex reaction path involving a potential well between reactants and products, leading to a bound adduct (or reaction complex) formed between the reactants A and B:

$$A + B \leftrightarrow [AB]^* \rightarrow C + D$$

The intermediate [AB]* is different from the transition state $[AB]^{\neq}$, in that it is a bound molecule which can, in principle, be isolated. (Of course, transition states are involved in all of the above reactions, both forward and backward, but are not explicitly shown.) An example of this reaction type is ClO + NO, which normally produces $Cl + NO_2$. Reactions of the nonconcerted type can have a more complex temperature dependence and can exhibit a pressure dependence if the lifetime of [AB]* is comparable to the rate of collisional deactivation of [AB]*. This arises because the relative rate at which [AB]* goes to products C + D vs. reactants A + B is a sensitive function of its excitation energy. Thus, in reactions of this type, the distinction between the bimolecular and termolecular classification becomes less meaningful, and it is especially necessary to study such reactions under the temperature and pressure conditions in which they are to be used in model calculation, or, alternatively, to develop a reliable theoretical basis for extrapolation of data.

The rate constant tabulation for second-order reactions (Table 1) is given in Arrhenius form:

k(T) = A exp ((-E/R)(1/T)) and contains the following information:

- Reaction stoichiometry and products (if known). The pressure dependences are included, where appropriate.
- Arrhenius A-factor.
- Temperature dependence and associated uncertainty ("activation temperature" E/R±ΔE/R).
- Rate constant at 298 K.
- Uncertainty factor at 298 K.
- Note giving basis of recommendation and any other pertinent information.

Uncertainty Estimates

For second-order rate constants in Table 1, an estimate of the uncertainty at any given temperature may be obtained from the following expression:

$$f(T) = f(298) \exp \left| \frac{\Delta E}{R} \left(\frac{1}{T} - \frac{1}{298} \right) \right|$$

Note that the exponent is an absolute value. An upper or lower bound (corresponding approximately to one standard deviation) of the rate constant at any temperature T can be obtained by multiplying or dividing the value of the rate constant at that temperature by the factor f(T). The quantity f(298) is the uncertainty in the rate constant at 298 K. ΔE/R is related to the uncertainty in the Arrhenius activation energy but is not strictly the one standard deviation uncertainty in the Arrhenius temperature coefficient. Rather, it has been defined in this evaluation for use with f(298) in the above expression to obtain the rate constant uncertainty at different temperatures.

This approach is based on the fact that rate constants are almost always known with minimum uncertainty at room temperature. The overall uncertainty normally increases at other temperatures, because there are usually fewer data and it is almost always more difficult to make measurements at other temperatures. It is important to note that the uncertainty at a temperature T cannot be calculated from the expression exp(ΔE/RT). The above expression for f(T) must be used to obtain the correct result.

The uncertainty represented by f(T) is normally symmetric; i.e., the rate constant may be greater than or less than the central value, k(T), by the factor f(T). In a few cases in Table 1 asymmetric uncertainties are given in the temperature coefficient. For these cases, the factors by which a rate constant is to be multiplied or divided to obtain, respectively, the upper and lower limits are not equal, except at 298 K where the factor is simply f(298 K). Explicit equations are given below for the case where the temperature dependence is (E/R +a, -b):

For T > 298 K, multiply by the factor

$$f(298\ K)e^{[a(1/298-1/T)]}$$

and divide by the factor

$$f(298\ K)e^{[b(1/298-1/T)]}$$

For T < 298 K, multiply by the factor

$$f(298\ K)e^{[b(1/T-1/298)]}$$

and divide by the factor

$$f(298\ K)e^{[a(1/T-1/298)]}$$

Examples of symmetric and asymmetric error limits are shown in Figure 1.

The assigned uncertainties represent the subjective judgment of the Panel. They are not determined by a rigorous, statistical analysis of the database, which generally is too limited to permit such an analysis. Rather, the uncertainties are based on a knowledge of the techniques, the difficulties of the experiments, and the potential for systematic errors.

There is obviously no way to quantify these "unknown" errors. The spread in results among different techniques for a given reaction may provide some basis for an uncertainty, but the possibility of the same, or compensating, systematic errors in all the studies must be recognized.

Furthermore, the probability distribution may not follow the normal Gaussian form. For measurements subject to large systematic errors, the true rate constant may be much further from the recommended value than would be expected based on a Gaussian distribution with the stated uncertainty. As an example, in the past the recommended rate constants for the reactions HO_2 + NO and Cl + $ClONO_2$ changed by factors of 30-50. These changes could not have been allowed for with any reasonable values of σ in a Gaussian distribution.

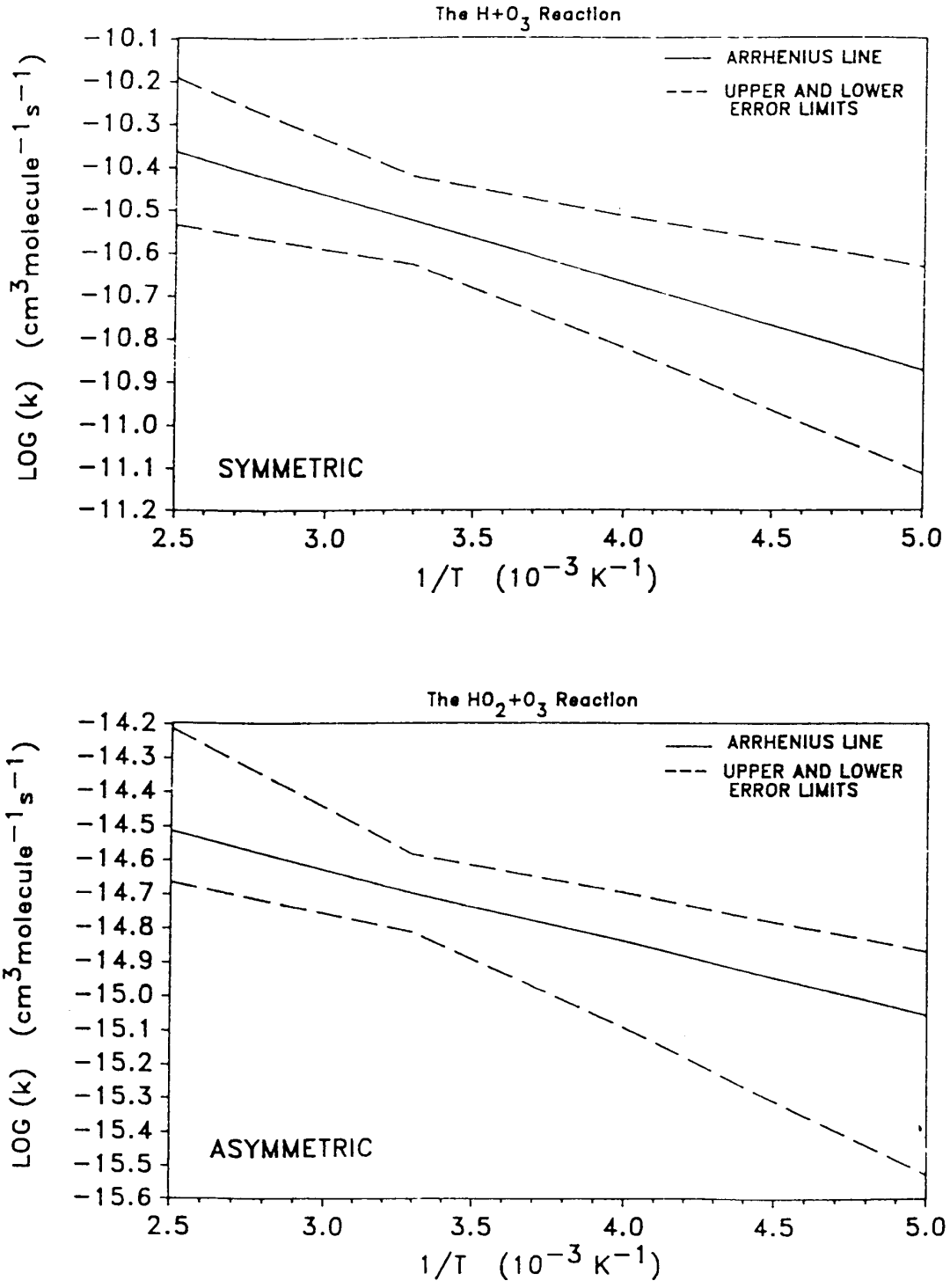

Figure 1: Symmetric and Asymmetric Error Limits

Table 1: Rate Constants for Second Order Reactions
(Shaded areas indicate changes or additions since the last version)

Reaction	A-Factor[a]	E/R±ΔE/R	k(298 K)[a]	f(298)[b]	Notes
<u>O(^{1}D) Reactions</u>					
$O(^1D) + H_2O \rightarrow OH + OH$	2.2×10^{-10}	0±100	2.2×10^{-10}	1.2	A6
$O(^1D) + N_2O \rightarrow N_2 + O_2$	4.9×10^{-11}	0±100	4.9×10^{-11}	1.3	A7
$\rightarrow NO + NO$	6.7×10^{-11}	0±100	6.7×10^{-11}	1.3	A7
<u>HO_X Reactions</u>					
$O + HO_2 \rightarrow OH + O_2$	3.0×10^{-11}	-(200±50)	5.9×10^{-11}	1.1	B 2
$OH + O_3 \rightarrow HO_2 + O_2$	1.5×10^{-12}	880±100	7.8×10^{-14}	1.2	B 6
$OH + HO_2 \rightarrow H_2O + O_2$	4.8×10^{-11}	-(250±100)	1.1×10^{-10}	1.3	B10
$HO_2 + O_3 \rightarrow OH + 2O_2$	2.0×10^{-14}	680 +200/-100	2.0×10^{-15}	1.2	B12
<u>NO_X Reactions</u>					
$O + NO_2 \rightarrow NO + O_2$	5.6×10^{-12}	-(180±50)	1.0×10^{-11}	1.1	C 1
$OH + HNO_3 \rightarrow H_2O + NO_3$	(See Note)			1.2	C 9
$NO + O_3 \rightarrow NO_2 + O_2$	3.0×10^{-12}	1500±200	1.9×10^{-14}	1.1	C20
<u>ClOx Reactions</u>					
$O + ClO \rightarrow Cl + O_2$	3.0×10^{-11}	-(70±70)	3.8×10^{-11}	1.15	F 1
$OH + ClO \rightarrow Cl + HO_2$	7.4×10^{-12}	-(270±100)	1.8×10^{-11}	1.4	F10
$\rightarrow HCl + O_2$	3.2×10^{-13}	-(320±150)	9.5×10^{-13}	3.0	F10
$OH + HCl \rightarrow H_2O + Cl$	2.6×10^{-12}	350±100	8.0×10^{-13}	1.1	F12
$Cl + O_3 \rightarrow ClO + O_2$	2.3×10^{-11}	200±100	1.2×10^{-11}	1.15	F49
$Cl + CH_4 \rightarrow HCl + CH3$	9.6×10^{-12}	1360±75	1.0×10^{-13}	1.05	F55
<u>BrOx Reactions</u>					
$BrO + ClO \rightarrow Br + OClO$	9.5×10^{-13}	-(550±150)	6.0×10^{-12}	1.25	G36
$\rightarrow Br + ClOO$	2.3×10^{-12}	-(260±150)	5.5×10^{-12}	1.25	G36
$\rightarrow BrCl + O_2$	4.1×10^{-13}	-(290±150)	1.1×10^{-12}	1.25	G36

a Units are cm^3 $molecule^{-1}$ s^{-1}

b f(298) is the uncertainty factor at 298 K. To calculate the uncertainty at other temperatures, use the expression:

$$f(T) = f(298)\exp\left|\frac{\Delta E}{R}\left(\frac{1}{T}-\frac{1}{298}\right)\right|$$

Note that the exponent is absolute value.

Notes to Table 1

A6. **$O(^1D) + H_2O$**. Measurements of the $O_2 + H_2$ product yield were made by Zellner et al. [356] (1 +0.5 or -1)% and by Glinski and Birks [117] (0.6 +0.7 or -0.6)%. The yield of $O(^3P)$ from $O(^1D) + H_2O$ is reported to be <(4.9±3.2)% by Wine and Ravishankara [346] and (2±1)% by Takahashi et al. [312].

To calculate the rates of OH production via $O(^1D)$ reactions in the atmosphere, the quantities of interest are the ratios of the rate coefficients for the reaction of $O(^1D)$ with H_2O to those with N_2 and with O_2. The ratios of the rate coefficients for $O(^1D)$ reactions measured using the same method (and often the same apparatus) are more accurate (and precise) than the individual rate constants that are quoted in Table 1. Ratio data are given in the original references for this reaction.

A7. **$O(^1D) + N_2O$**. The branching ratio for the reaction of $O(^1D)$ with N_2O to give $N_2 + O_2$ or NO + NO is an average of the values reported by Davidson et al. [78]; Volltrauer et al. [333]; Marx et al. [213] and Lam et al. [190], with a spread in R=k(NO + NO)/k(Total) = 0.52 - 0.62. Cantrell et al. [55] reported a measurement of R=0.57 and an analysis of all measurements from 1957-1994 leads them to recommend a value of R=0.61±0.06, where the uncertainty indicates their 95% confidence interval. The recommended branching ratio agrees well with earlier measurements of the quantum yield from N_2O photolysis (Calvert and Pitts [52]). The $O(^1D)$ translational energy and temperature dependence effects are not clearly resolved. Wine and Ravishankara [346] have determined that the yield of $O(^3P)$ from $O(^1D) + N_2O$ is <4.0%. The uncertainty for this reaction includes factors for both the overall rate coefficient and the branching ratio. A direct measurement by Greenblatt and Ravishankara [119] of the NO yield from the $O(^1D) + N_2O$ reaction in synthetic air agrees very well with the value predicted using the recommended $O(^1D)$ rate constants for N_2, O_2, and N_2O and the $O(^1D) + N_2O$ product branching ratio. These authors suggest that their results support the recommendations and reduce the uncertainty in the collected rate parameters by over a factor of two.

To calculate the rates of NO production via $O(^1D)$ reactions in the atmosphere, the quantities of interest are the ratios of the rate coefficients for the reaction of $O(^1D)$ with N_2O to those with N_2 and with O_2. The ratios of the rate coefficients for $O(^1D)$ reactions measured using the same method (and often the same apparatus) are more accurate and precise than the individual rate constants that are quoted in Table 1. Ratio data are given in the original references for this reaction.

B2. **$O + HO_2$**. The recommended values are based on the results of studies over a range of temperatures by Keyser [170] and Nicovich and Wine [236] and the room temperature studies of Sridharan et al. [301], Ravishankara et al. [264], and Brune et al. [39]. Earlier studies by Hack et al. [121] and Burrows et al. [44,46] are not considered, because the OH + H_2O_2 reaction was important in these studies and the value used for its rate constant in their analyses has been shown to be in error. Data from Ravishankara et al. [264] at 298 K show no dependence on pressure between 10 and 500 torr N_2. The ratio $k(O + HO_2)/k(O + OH)$ measured by Keyser [171] agrees with the rate constants recommended here. Sridharan et al.

[299] showed that the reaction products correspond to abstraction of an oxygen atom from HO_2 by the O reactant. Keyser et al. [174] reported <1% $O_2(^1\Delta)$ yield.

B6. **$OH + O_3$**. Recommended values are based on the results of studies over a range of temperatures by Ravishankara et al. [263] and Smith et al. [294] and the room temperature measurements of Kurylo [187], Zahniser and Howard [352], and Kulcke et al. [186]. In the study of Kulcke et al. [186] the two rate constants sum, $k(OH + O_3) + k(HO_2 + O_3)$, which is dominated by the first term, was determined to be $(8.4 \pm 0.8) \times 10^{-14}$ cm^3 $molecule^{-1}$ s^{-1}.

B10. **$OH + HO_2$**. A study by Keyser [173] appears to resolve a discrepancy between low-pressure discharge flow experiments that all gave rate coefficients near 7×10^{-11} cm^3 $molecule^{-1}$ s^{-1} : Keyser [169], Thrush and Wilkinson [318], Sridharan et al. [300,302], Temps and Wagner [315], and Rozenshtein et al. [274], and atmospheric pressure studies that gave rate coefficients near 11×10^{-11}: Lii et al. [201], Hochanadel et al. [148], DeMore [82], Cox et al. [71], Burrows et al. [45], and Kurylo et al. [189]. Laboratory measurements using a discharge flow experiment and a chemical model analysis of the results by Keyser [173] demonstrate that the previous discharge flow measurements were probably subject to interference from small amounts of O and H. In the presence of excess HO_2 these atoms generate OH and result in a rate coefficient measurement that falls below the true value.

The temperature dependence is from Keyser [173], who covered the range 254 to 382 K. A flow tube study by Schwab et al. [283] reported $k = (8.0 +3/-4) \times 10^{-11}$. These workers measured the concentrations of HO_2, OH, O, and H and used a computer model of the relevant reactions to test for interference. A flow tube study by Dransfeld and Wagner [100] employing an isotope labelled ^{18}OH reactant obtained $k = (11\pm2) \times 10^{-11}$ in good agreement with the recommendation. They attributed about half of the reactive events to isotope scrambling because control experiments with ^{16}OH gave $k = 6 \times 10^{-11}$. It should be noted that their control experiments were subject to the errors described by Keyser [173] due to the presence of small amounts of H and O, whereas their ^{18}OH measurements were not. Kurylo et al. [189] found no evidence of significant scrambling in isotope studies of the OH and HO_2 reaction. An additional careful study of the reaction temperature dependence would be useful. Hippler and Troe [146] have analysed data for this reaction at temperatures up to 1250K. In summary, this has historically been a difficult reaction to study. Earlier problems appear to have been resolved, as discussed above, and results now tend to converge on a central value, but the recommended value is still subject to a large uncertainty.

B12. **$HO_2 + O_3$**. The recommended values are based on results of studies over a range of temperatures by Zahniser and Howard [352] at 245 to 365 K, Manzanares et al. [210] at 298 K, Sinha et al. [291] at 243 to 413 K, Wang et al. [337] at 233 to 400 K and the steady-state photolysis experiments of DeMore [80] at 231 to 334 K. The temperature dependence studies show varying degrees of curvature in the Arrhenius plots, with the E/R decreasing at lower temperature. However, the fit to data in the stratospherically relevant 230 K to 300 K range is not significantly affected by inclusion of higher temperature data in the recommendation. Additional temperature dependence data are needed for this reaction to more fully characterize the non-linear behavior of the rate constant at low temperature. The mechanism of the reaction has been studied using ^{18}O labelled HO_2 by Sinha et al. [291], who

reported that the reaction occurs 75±10% via H atom transfer at 297K and by Nelson and Zahniser [233], who reported branching ratios for H transfer vs O transfer over the range 226-355K. They report that the H atom transfer decreases from 94±5% at 226±11K to 88±5% at 355±8K.

C1. **$O + NO_2$**. The recommended values are based on the results of studies over a range of temperatures by Gierczak et al. [116], Ongstad and Birks [239], Slanger et al. [292] and Geers-Muller and Stuhl [114] and the room temperature study of Paulson et al. [246]. In the most recent study of Gierczak et al. [116], special emphasis was placed on accurate measurement of the NO_2 concentration and on measurements at low temperatures. The results of earlier studies by Davis et al. [79] and Bemand et al. [28] were not used in deriving the recommended values either because of possible complications from decomposition of NO_2 at higher temperatures or lack of direct NO_2 detection.

C9. **$OH + HNO_3$**. The recent study of Brown et al. [38] furnishes the most comprehensive set of rate measurements for N_2 as the bath gas over a significant range of temperature (200-350 K) and pressure (20-500 torr). They analyzed their results in terms of the mechanism proposed by Smith et al. [294], involving the formation of a bound, relatively long-lived $HO{\cdot}HNO_3$ complex, as well as the direct reaction channel. Thus, the P dependence can be represented by combining a low pressure (bimolecular) limit, k_0, with a Lindemann-Hinshelwood expression for the p-dependence:

$$k([M],T)=k_o+\frac{k_3[M]}{1+\frac{k_3[M]}{k_2}} \qquad \left\{\begin{aligned} k_o &= 2.4x10^{-14}\exp(460/T) \\ k_2 &= 2.7x10^{-17}\exp(2199/T) \\ k_3 &= 6.5x10^{-34}\exp(1335/T) \end{aligned}\right\}$$

The coefficients k_3 and k_2 are the termolecular and high pressure limits for the "association" channel. The value of k at high pressures is the sum $k_0 + k_2$.

This expression for k([M],T) and the values of the Arrhenius parameters for k_0, k_2, and k_3 derived by Brown et al. [38] for N_2 as the bath gas constitute the recommended values for this rate coefficient. These recommended values are derived from a fit to the data of Brown et al. [38], Stachnik et al. [303], Devolder et al. [96] and Margitan and Watson [212].

The reaction as written assumes that the yield of NO_3 (per OH removed) is unity at all temperatures and that the yield has the same value for both reaction channels. However, a reanalysis of previously published data leads to NO_3 yields of 0.75 at 298 K and 0.89 at 251 K (Brown et al. [38]). Better quantification of this yield as a function of pressure and temperature is needed.

C20. **$NO + O_3$**. The recommended values are based on the results of studies over a range of temperatures by Birks et al. [33], Lippmann et al. [204], Ray and Watson [267], Michael et al. [216], Borders and Birks [34] and Moonen et al. [228] and the room temperature studies of Stedman and Niki [306] and Bemand et al. [28]. The six temperature-dependent studies were given equal weighting in the recommendation by averaging over the E/R's from each individual data set. Following the Moonen et al. recommendation, the 200 K data point from their study has been excluded from the fit. All of the temperature dependence studies show some curvature in the Arrhenius plot at temperatures below 298K. Increasing scatter between the data sets is evident at the lower temperatures. Clough and Thrush [63], Birks et al., Schurath et al. [282], and Michael et al. have reported individual Arrhenius parameters for the two primary reaction channels producing ground and excited molecular oxygen.

F1. **O + ClO**. There have been five studies of this rate constant over an extended temperature range using a variety of techniques: Leu [194]; Margitan [211]; Schwab et al. [284]; Ongstad and Birks [239]; and Nicovich et al. [237]. The recommended value is based on a least squares fit to the data reported in these studies and in the earlier studies of Zahniser and Kaufman [353] and Ongstad and Birks [238]. Values reported in the early studies of Bemand et al. [27] and Clyne and Nip [64] are significantly higher and were not used in deriving the recommended value. Leu and Yung [200] were unable to detect $O_2(^1\Delta)$ or $O_2(^1\Sigma)$ and set upper limits to the branching ratios for their production of 4.4×10^{-4} and 2.5×10^{-2} respectively.

F10. **OH + ClO**. The reaction has two known product channels under atmospheric conditions: $OH + ClO \rightarrow Cl + HO_2$ and $OH + ClO \rightarrow HCl + O_2$. Most studies measure the rate coefficients for the overall reaction ($OH + ClO \rightarrow$ products) which is presumably the sum of the two channels. The recommendation for the $Cl + HO_2$ channel is obtained from the difference between a critical assessment of the measurements of the overall reaction and the recommendation for the $HCl + O_2$ channel. The assessment of the overall reaction ($OH + ClO \rightarrow$ products) is based on a fit to the 219-373 K data of Hills and Howard [144], the 208-298 K data of Lipson et al. [206], the 234-356 K data of Kegley-Owen et al. [167] and the 298 K data of Poulet et al. [252]. Data reported in the studies of Burrows et al. [50], Ravishankara et al. [260], and Leu and Lin [197] were not used in deriving the recommended value because ClO was not measured directly in these studies and the concentration of ClO was determined by an indirect method. The fraction of total reaction yielding $HO_2 + Cl$ as products has been determined by Leu and Lin (>0.65); Burrows et al. (0.85±0.2); Hills and Howard (0.86±0.14); and Poulet et al. (0.98±0.12). Temperature-dependent rate constants for the $HCl + O_2$ channel have been directly measured by Lipson et al. [205] by observing the HCl product and the recommendation is based on this work.

F12. **OH + HCl**. The recommended value is based on a least squares fit to the data over the temperature range 240-300 K reported in the studies by Molina et al. [225], Keyser [172], Ravishankara et al. [265] and Battin-Leclerc et al. [23]. In these studies particular attention was paid to the determination of the absolute concentration of HCl by UV and IR spectrophotometry. Earlier studies by Takacs and Glass [308], Zahniser et al. [354], Smith and Zellner [298], Ravishankara et al. [261], Hack et al. [120], Husain et al. [156], Cannon et al. [53], Husain et al. [157], and Smith and Williams [297] had reported somewhat lower room temperature values. The data of Sharkey and Smith [288] over the temperature range 138-216 K and Battin-Leclerc et al. [23] below 240 K depart from normal Arrhenius behavior. It is unknown whether this is due to an effect such as tunneling at low temperature or a systematic experimental error. Additional work at low temperature is needed.

F49. **$Cl + O_3$**. The results reported for k(298 K) by Watson et al. [342], Zahniser et al. [355], Kurylo and Braun [188], Clyne and Nip [65], Nicovich et al. [235] and Seeley et al. [287] are in good agreement, and have been used to determine the preferred value at this temperature. The values reported by Leu and DeMore [196] (due to the wide error limits) and Clyne and Watson [67] (the value is inexplicably high) are not considered. The six Arrhenius expressions are in fair agreement within the temperature range 205-300 K. In this temperature range, the rate constants at any particular temperature agree to within 30-40%. Although the values of the activation energy obtained by Watson et al. and Kurylo and Braun are in excellent agreement, the value of k in the study of Kurylo and Braun is consistently (~17%) lower than that of Watson et al. This may suggest a systematic underestimate of the rate constant, as the values from the other three agree so well at 298 K. The two most recent studies (Nicovich et al. and Seeley et al.) obtained significantly smaller temperature dependences than those observed in the earlier studies. There is no reason to prefer any one set of data to any other; therefore, the preferred Arrhenius expression shown above was obtained by computing the mean of the six results between 205 and 298 K. DeMore [83] directly determined the ratio $k(Cl + O_3)/k(Cl + CH_4)$ at 197-217 K to be within 15% of that calculated from the absolute rate constant values recommended here.

Vanderzanden and Birks [330] have interpreted their observation of oxygen atoms in this system as evidence for some production (0.1-0.5%) of O_2 ($^1\Sigma_g^+$) in this reaction. The possible production of singlet molecular oxygen in this reaction has also been discussed by DeMore [81], in connection with the Cl_2 photosensitized decomposition of ozone. However Choo and Leu [60] were unable to detect $O_2(^1\Sigma)$ or $O_2(^1\Delta)$ in the $Cl + O_3$ system and set upper limits to the branching ratios for their production of 5×10^{-4} and 2.5×10^{-2}, respectively. They suggested two possible mechanisms for the observed production of oxygen atoms, involving reactions of vibrationally excited ClO radicals with O_3 or with Cl atoms, respectively. Burkholder et al. [42], in a study of infrared line intensities of the ClO radical, present evidence in support of the second mechanism. In their experiments with excess Cl atoms, the vibrationally excited ClO radicals produced in the $Cl + O_3$ reaction can react with Cl atoms to give Cl_2 and oxygen atoms, which can then remove additional ClO radicals. These authors point out the possibility for systematic error from assuming a 1:1 stoichiometry for $[Cl]:[O_3]_0$ when using the $Cl + O_3$ reaction as a quantitative source of ClO radicals for kinetic and spectroscopic studies.

F55. **$Cl + CH_4$**. The values of k at 298 K reported from thirteen absolute rate constant studies (Manning and Kurylo [209], Whytock et al. [343], Michael and Lee [217], Lin et al. [203], Zahniser et al. [350], Keyser [168], Ravishankara and Wine [262], Heneghan et al. [140], Dobis and Benson [97], Sawerysyn et al. [279], Beichert et al. [26], Seeley et al. [287], and Pilgrim et al. [250]) fall in the range (0.92 - 1.13) x 10^{-13}, with a mean value of 0.99 x 10^{-13}. An earlier absolute study by Watson et al. [342] gives rate constant values slightly higher than those of the aforementioned studies, which may be due to uncertainties in correcting the data for OH loss via reaction with trace levels of ethane and propane in the methane samples used.

The values derived for k at 298 K from the competitive chlorination studies of Pritchard et al. [255], Pritchard et al. [256], Knox [183], Knox and Nelson [184], Lee and Rowland [191], and Lin et al. [203] range from (0.8 - 1.6) x 10^{-13} when the original data are referenced to the presently recommended rate constant values for the reactions of Cl with H_2 and C_2H_6. Of these relative rate studies, that of Lin et al. [203], yields a room temperature rate constant (1.07 x 10^{-13}) that is most consistent with the absolute measured values. Thus, the recommended value for k at 298K (1.0 x 10^{-13}) is derived from an unweighted average of the rate constants from the thirteen preferred absolute studies and the relative rate study of Lin et al. [203].

There have been nine absolute studies of the temperature dependence of k in which the measurements extend below 300K (Watson et al. [342], Manning and Kurylo [209], Whytock et al. [343], Lin et al. [203], Zahniser et al. [350], Keyser [168], Ravishankara and Wine [262], Heneghan et al. [140], and Seeley et al. [287]). In general, the agreement among most of these studies is quite good. However, systematic differences in activation energies are apparent when calculated using data obtained below 300K versus data from above 300K. Three resonance fluorescence studies have been performed over the temperature region between 200K and 500K (Whytock et al. [343], Zahniser et al. [350] and Keyser [168]), and in each case a strong nonlinear Arrhenius behavior was observed. Ravishankara and Wine [262] also noted nonlinear Arrhenius behavior over a more limited temperature range. This behavior tends to partially explain the variance in the values of E/R reported between those investigators who mainly studied this reaction below 300 K (Watson et al. [342], Manning and Kurylo [209], and Seeley et al. [287])] and those who only studied it above 300 K (Clyne and Walker [66], Poulet et al. [253], and Lin et al. [203]). The agreement among all studies below 300 K is reasonably good, with values of E/R ranging from (1063 - 1320)K, and k(230K) in the range (2.6 - 3.2) x 10^{-14}. There have not been any absolute studies at stratospheric temperatures other than those which utilized the resonance fluorescence technique. Ravishankara and Wine [262] have suggested that the results obtained using the discharge flow and competitive chlorination techniques may be in error at the lower temperatures (<240 K) due to a non-equilibration of the $^2P_{1/2}$ and $^2P_{3/2}$ states of atomic chlorine. Ravishankara and Wine observed that at temperatures below 240K the apparent bimolecular rate constant was dependent upon the chemical composition of the reaction mixture; i.e., if the mixture did not contain an efficient spin equilibrator, e.g., Ar or CCl_4, the bimolecular rate constant decreased at high CH_4 concentrations. The chemical composition in each of the flash photolysis studies contained an efficient spin equilibrator, whereas this was not the case in the discharge flow studies. However, the reactor walls in the discharge flow studies could have been expected to have acted as an efficient spin equilibrator. Consequently, until the hypothesis of Ravishankara and Wine is proven it is assumed that the discharge flow and competitive chlorination results are reliable. A

composite unweighted Arrhenius fit to all of the temperature dependent absolute studies with data in the temperature region ≤300K (with the exception of the data of Watson et al. [342], which appear to be systematically high due to reactive impurities) yields E/R = 1253K and k(298K) = 1.0 x 10^{-13}.

The competitive chlorination results differ from those obtained in the absolute studies in that linear Arrhenius behavior is observed. The values of E/R are consistently larger than those obtained from the absolute studies, with an average value of approximately 1500K. Until the hypothesis of Ravishankara and Wine [262] is re-examined, the preferred Arrhenius expression attempts to best fit the results obtained between 200 and 300 K from all sources. Thus, using the relative rate results of Lin et al. [203] (referenced to the current recommendation for the Cl + C_2H_6 reaction) as representative of the relative rate studies below 300K, together with the composite fit to the absolute studies given above, we obtain a recommended E/R value of 1360K. Taken with the recommended value for k(298K) = 1.0 x 10^{-13}, we compute an Arrhenius A factor of 9.6 x 10^{-12}. However, the A-factor thus derived seems somewhat low (on a per hydrogen atom basis) when compared with the A-factors for some similar reactions.

G36. **BrO + ClO**. Friedl and Sander [112], using DF/MS techniques, measured the overall rate constant over the temperature range 220-400 K and also over this temperature range determined directly branching ratios for the reaction channels producing BrCl and OClO. The same authors in a separate study using flash photolysis-ultraviolet absorption techniques (Sander and Friedl [276]) determined the overall rate constant over the temperature range 220-400 K and pressure range 50-750 torr and also determined at 220 K and 298 K the branching ratio for OClO production. The results by these two independent techniques are in excellent agreement, with the overall rate constant showing a negative temperature dependence. Toohey and Anderson [321], using DF/RF/LMR techniques, reported room temperature values of the overall rate constant and the branching ratio for OClO production. They also found evidence for the direct production of BrCl in a vibrationally excited Π state. Poulet et al. [251], using DF/MS techniques, reported room temperature values of the overall rate constant and branching ratios for OClO and BrCl production. Overall room temperature rate constant values reported also include those from the DF/MS study of Clyne and Watson [68] and the very low value derived in the flash photolysis study of Basco and Dogra [21] using a different interpretation of the reaction mechanism. The recommended Arrhenius expressions for the individual reaction channels are taken from the study of Friedl and Sander [112] and Turnipseed et al. [327] . These studies contain the most comprehensive sets of rate constant and branching ratio data. The overall rate constants reported in these two studies are in good agreement (20%) at room temperature and in excellent agreement at stratospheric temperatures. Both studies report that OClO production by channel (1) accounts for 60% of the overall reaction at 200 K. Both studies report a BrCl yield by channel (3) of about 8%, relatively independent of temperature. The recommended expressions are consistent with the body of data from all studies except those of Hills et al. [143] and Basco and Dogra [21].

TERMOLECULAR REACTIONS

Rate constants for third order reactions (Table 2) of the type A + B $\rightleftarrows$ [AB]* $\xrightarrow{M}$ AB are given in the form:

$$k_o(T) = k_o^{300}\left(\frac{T}{300}\right)^{-n} \text{ cm}^6 \text{ molecule}^{-2} \text{ s}^{-1},$$

(where k_o^{300} has been adjusted for air as the third body), together with a recommended value of n. Where pressure fall-off corrections are necessary, an additional entry gives the limiting high-pressure rate constant in a similar form:

$$k_\infty(T) = k_\infty^{300}\left(\frac{T}{300}\right)^{-m} \text{ cm}^3 \text{ molecule}^{-1} \text{ s}^{-1}.$$

To obtain the effective second-order rate constant for a given condition of temperature and pressure (altitude), the following formula is used:

$$k_f([M],T) = \left(\frac{k_o(T)[M]}{1+\frac{k_o(T)[M]}{k_\infty(T)}}\right) 0.6^{\left\{1+\left[\log_{10}\left(\frac{k_o(T)[M]}{k_\infty(T)}\right)\right]^2\right\}^{-1}}$$

The fixed value 0.6 that appears in this formula fits the data for all listed reactions adequately, although in principle this quantity may be different for each reaction, and also temperature dependent.

Thus, a compilation of rate constants of this type requires the stipulation of the four parameters, $k_O(300)$, n, $k_\infty(300)$, and m. These can be found in Table 2. The discussion that follows outlines the general methods we have used in establishing this table, and the notes to the table discuss specific data sources.

Low-Pressure Limiting Rate Constant [$k_0^x(T)$]

Troe [323] has described a simple method for obtaining low-pressure limiting rate constants. In essence this method depends on the definition:

$$k_o^x(T) \equiv \beta_x k_{o,sc}^x$$

Here sc signifies "strong" collisions, x denotes the bath gas, and β_x is an efficiency parameter ($0 < \beta_x < 1$), which provides a measure of energy transfer.

The coefficient β_X is related to the average energy transferred in a collision with gas x, $\langle\Delta E\rangle_X$, via:

$$\frac{\beta_x}{\left(1-\sqrt{\beta_x}\right)} = \frac{\langle\Delta E\rangle_x}{F_E kT}$$

Notice that $<\Delta E>$ is quite sensitive to ß. F_E is the correction factor of the energy dependence of the density of states (a quantity of the order of 1.1 for most species of stratospheric interest).

For some of the reactions of possible stratospheric interest reviewed here, there exist data in the low-pressure limit (or very close thereto), and we have chosen to evaluate and unify this data by calculating $k_o^x(T)$ for the appropriate bath gas x and computing the value of $ß_x$ corresponding to the experimental value [Troe [323]]. A compilation (Patrick and Golden [245]) gives details for many of the reactions considered here.

From the ßx values (most of which are for N_2, i.e., $ß_{N2}$), we compute $<\Delta E>_X$ according to the above equation. Values of $<\Delta E>_{N2}$ of approximately 0.3-1 kcal $mole^{-1}$ are generally expected. If multiple data exist, we average the values of $<\Delta E>_{N2}$ and recommend a rate constant corresponding to the $ß_{N2}$ computed in the equation above.

Where no data exist we have sometimes estimated the low-pressure rate constant by taking $ß_{N2} = 0.3$ at T = 300 K, a value based on those cases where data exist.

Temperature Dependence of Low-Pressure Limiting Rate Constants: T^n

The value of n recommended here comes from measurements or, in some cases, a calculation of $<\Delta E>_{N2}$ from the data at 300 K, and a computation of $ß_{N2}$ (200 K) assuming that $<\Delta E>_{N2}$ is independent of temperature in this range. This $ß_{N2}$ (200 K) value is combined with the computed value of k_o^{sc} (200 K) to give the expected value of the actual rate constant at 200 K. This latter, in combination with the value at 300 K, yields the value of n.

This procedure can be directly compared with measured values of k_o (200 K) when those exist. Unfortunately, very few values at 200 K are available. There are often temperature-dependent studies, but some ambiguity exists when one attempts to extrapolate these down to 200 K. If data are to be extrapolated beyond the measured temperature range, a choice must be made as to the functional form of the temperature dependence.

There are two general ways of expressing the temperature dependence of rate constants. Either the Arrhenius expression

$$k_O(T) = A\exp(-E/RT) \text{ or the form } k_O(T) = A' T^{-n}$$

is employed. Since neither of these extrapolation techniques is soundly based, and since they often yield values that differ substantially, we have used the method explained earlier as the basis of our recommendations.

High-Pressure Limit Rate Constants [$k_\infty(T)$]

High-pressure rate constants can often be obtained experimentally, but those for the relatively small species of atmospheric importance usually reach the high-pressure limit at inaccessibly high pressures. This leaves two sources of these numbers, the first being guesses based upon some model, and the second being extrapolation of fall-off data up to higher pressures.

Stratospheric conditions generally render reactions of interest much closer to the low-pressure limit and thus are fairly insensitive to the high-pressure value. This means that while the extrapolation is long, and the value of $k_\infty(T)$ not very accurate, a "reasonable guess" of $k_\infty(T)$ will then suffice. In some cases we have declined to guess since the low-pressure limit is effective over the entire range of stratospheric conditions.

Temperature Dependence of High-Pressure Limiting Rate Constants: T^m

There are very few data upon which to base a recommendation for values of m. Values in Table 2 are often estimated, based on models for the transition state of bond association reactions and whatever data are available.

Uncertainty Estimates

For three-body reactions (Table 2) uncertainties are assigned using a procedure that is analogous to that employed for bimolecular reactions. Uncertainties expressed as increments to k_o and k_∞ are given for these rate constants at room temperature. The additional uncertainty arising from the temperature extrapolation is expressed as an uncertainty in the temperature coefficients n and m.

Table 2: Rate Constants for Association Reactions
(Shaded areas indicate changes or additions since the last version)

Reaction	Low Pressure Limit[a] $k_o(T) = k_o^{300}(T/300)^{-n}$		High Pressure Limit[b] $k_\infty(T) = k_\infty^{300}(T/300)^{-m}$		Notes
	k_o^{300}	n	k_∞^{300}	m	
$O + O_2 \xrightarrow{M} O_3$	(6.0±0.5) (-34)	2.4±0.2			A1
$O + NO \xrightarrow{M} NO_2$	(9.0±2.0) (-32)	1.5±0.3	(3.0±1.0) (-11)	0±1.0	C1
$OH + NO_2 \xrightarrow{M} HONO_2$	(2.4±0.1) (-30)	3.1±0.2	(1.7±0.2) (-11)	2.1±0.3	C4
$NO_2 + NO_3 \xrightarrow{M} N_2O_5$	(2.0±0.2) (-30)	4.4±0.4	(1.4±0.1) (-12)	0.7±0.4	C6
$ClO + NO_2 \xrightarrow{M} ClONO_2$	(1.8±0.3) (-31)	3.4±0.2	(1.5±0.4) (-11)	1.9±0.5	F8
$ClO + ClO \xrightarrow{M} Cl_2O_2$	(2.2±0.2) (-32)	3.1±0.2	(3.4±0.5) (-12)	1.0±1	F10
$BrO + NO_2 \xrightarrow{M} BrONO_2$	(5.2±0.4) (-31)	3.2±0.8	(6.9±0.4) (-12)	2.9±0.1	G2

$$k_f([M],T) = \left(\frac{k_o(T)[M]}{1 + \left(\frac{k_o(T)[M]}{k_\infty(T)} \right)} \right) 0.6^{\left\{ 1 + \left[\log_{10}\left(\frac{k_o(T)[M]}{k_\infty[T]} \right) \right]^2 \right\}^{-1}}$$

The values quoted are suitable for air as the third body, M.

a Units are cm^6 $molecule^{-2}$ s^{-1}.

b Units are cm^3 $molecule^{-1}$ s^{-1}.

Notes to Table 2

A1. **$O + O_2$**. Temperature dependence re-evaluated. Low pressure limit and T dependence are an average of Klais, Anderson, and Kurylo [180] and Lin and Leu [202]. The result is in agreement with most previous work (see references therein) and with the study of Hippler et al. [Hippler, 1990 #55. Kaye [166] has calculated isotope effects for this reaction, using methods similar to those discussed in the Introduction (Troe [323], Patrick and Golden [245].) Croce de Cobos and Troe [75] are in agreement with earlier work. Rawlins et al. [266] report values in Ar between 80 and 150K that extrapolate to agreement with the recommended values.

C1. **O + NO**. Low pressure limit and n from direct measurements of Schieferstein et al. [280] and their re-analysis of the data of Whytock et al. [344]. Error limits encompass other studies. High pressure limit and m from Baulch et al. [25] and Baulch et al. [24], slightly modified. Hippler et al. [145] report higher values for the high pressure limiting rate constant. Atkinson et al. [12] use F_c =exp(-T/1850). This yields rate constants 10-20% higher than obtained from Table 2. Shock tube measurements by Yarwood et al. [349] in argon from 300-1300K are consistent with the values in Table 2.

C4. **$OH + NO_2$**. The low pressure limit and the high pressure limiting rate constants and their temperature dependences are from a weighted fit to the data of Anastasi and Smith [8], Wine et al. [345] and Dohahue et al. [98]. (The values reported in JPL 97-4 used the same data without weighting, accounting for the different temperature dependence of the low pressure limit.) Data reported in 1999 by Dransfield et al. [101] and Brown et al. [37] are in excellent agreement. (Brown et al. report that O_2 is about 30% less efficient than N_2 as a collider and suggest that air might therefore have a total efficiency of 0.94 relative to N_2) Data from Anderson et al. [9], Howard and Evenson [151], Burrows et al. [49], and Erler et al. [105] are in essential agreement. Data of Forster et al [107] and Fulle et al. [113] appear to be too high. These results and those of Robertshaw and Smith [269], who have measured k in up to 8.6 atmospheres of CF_4, suggest that k_∞ might be higher than suggested here. This disagreement might also be due to other causes (i.e., the failure of the simplified fall-off expression as suggested by Donahue et al., isomer formation, or involvement of excited electronic states). Burkholder et al. [41] searched for the isomer HOONO and were unable to measure it. RRKM calculations suggest that the lifetime of the latter species may be too short to observe under their conditions (248-298 K, 3-850 Torr), but long enough to interfere with the very high pressure results of Forster et al. [107] and Fulle et al. [113]. The temperature dependence of both limiting rate constants [345] is consistent with Smith and Golden [296] and Patrick and Golden [245]. The recommendation here fits all data over the range of atmospheric interest.

The data of Forster et al. [107] and Fulle et al. [113] may represent the sum of the pathways forming $HONO_2$ and HOONO. Those experiments were performed on timescales rapid enough to preclude the dissociation of the HOONO isomer. RRKM calculations [Golden, D. M., and G. P. Smith submitted to J. Phys. Chem.] calibrated in accord with this postulate lead to the conclusion that the low temperature laboratory data also measure the sum of the two pathways. Deconvoluting the data yields a rate constant for nitric acid formation at stratospheric temperatures that is lower than computed from the Table 2 values.

This can be entered into models using parameters that describe the individual steps as given below.

Fits to individual product species in Table 2 format:

$HONO_2$: $k_o(300) = 2.40x10^{-30}$; n = 2.6; $k_\infty(300) = 1.8x10^{-11}$; m = 0.1
HOONO: $k_o(300) = 2.30x10^{-31}$; n = 3.1; $k_\infty(300) = 7.3x10^{-11}$; m = 1.3

For the HOONO case, the reverse reaction must be taken into account through the equilibrium constant. In the format of Table 3:

$A=1.2x10^{-26}$; B = 8260, K(298K) = $1.3x10^{-14}$ and f(298K) = 10

The parameters relating to HOONO are provided for the purposes of model evaluation only and are not part of the Panel's recommendation for reaction C4.

C6. **$NO_2 + NO_3$**. Data with N_2 as the bath gas from Kircher et al. [179], Smith et al. [295], Burrows et al. [48], Wallington et al. [335] and Orlando et al. [243] ranging from 236 to 358K were used to obtain k_0, k_∞, n and m. Values from Croce de Cobos et al. [75] are excluded due to arguments given by Orlando et al. [243], who point out that a reanalysis of these data using better values for the rate constant for $NO_3 + NO \rightarrow 2NO_2$ yields a negative value for $NO_2 + NO_3 + M$. The study of Fowles et al. [108] is noted, but not used. Johnston et al. [163] have reviewed this reaction.

A study of the reverse reaction has been carried out by Cantrell et al. [56]. These data are in excellent agreement with those obtained by Connell and Johnston [69] and Viggiano et al. [331]. The equilibrium constant recommended in Table 3 is in excellent agreement with the one given in Cantrell et al. [56], who computed it from the ratio of the rate constant of Orlando et al. [243] and their rate constants for the reverse reaction.

F8. **$ClO + NO_2$**. The low pressure limit recommendation and uncertainties are based on temperature dependent values from Zahniser et al. [351], Lee et al. [193], Birks et al. [32], Leu et al. [198], Wallington and Cox [336], Cox et al. [70] and Molina et al. [224]. All of these data were collected in N_2 bath gas, except for several points from Lee et al. [193] collected in O_2.

The high pressure limit recommendation is based on the RRKM calculations of Smith and Golden . There are several pressure dependent data sets in the literature, such as Percival et al. [247], Handwerk and Zellner [122], Dasch et al. [77] and Cox and Lewis [74]; however, they are too disparate to extract unambiguous values. These data are all reproduced within two sigma error limits by the current recommendation.

F10. **ClO + ClO**. The recommendation is based on a simultaneous fit to data from Sander et al. (194 - 247 K) [275], Nickolaisen et al. (260 - 390 K) [234], and Trolier et al. (200 - 263 K) [324], holding m fixed at 1.0. Latter data have been corrected for the effect of Cl_2 as third body, as suggested by Nickolaisen et al. With this adjustment all the data are in good agreement. Error limits are from the statistical fit. The k_O value for N_2 is not in accord with a Patrick and Golden-type calculation [245]. This may be due to uncertainty in the ClOOCl thermochemistry, which is based on the equilibrium constants reported by Nickolaisen et al. and Cox and Hayman [59] (See Table 3). Other previous rate constant measurements, such as those of Hayman et al. [139], Cox and Derwent [72], Basco and Hunt [22], Walker [334], and Johnston et al. [164], range from 1-5 x 10^{-32} cm^6 $molecule^{-2}$ s^{-1}, with N_2 or O_2 as third bodies. The major dimerization product is chlorine peroxide (Birk et al. [31], DeMore and Tschuikow-Roux [94], Slanina and Uhlik [293], Stanton et al. [305] and Lee et al. [192]).

G2. **BrO + NO_2**. Values from a study by Thorn et al. [317] that is in excellent agreement with Sander et al. [278] are recommended. Error limits are from a reanalysis of the data. Danis et al. [76] give slightly lower values for the low pressure limiting rate constant and a smaller temperature dependence as well. This latter study may be hampered by heterogeneous effects. A theoretical study by Rayez and Destriau [268] suggests that the bond dissociation energy in $BrONO_2$ is higher than that in $ClONO_2$, thus rationalizing the relative values of the low pressure limiting rate constants for these two processes. This is confirmed by a more detailed study by Parthiban and Lee. [244] as well as by Orlando and Tyndall [242], who measured $BrONO_2$ decomposition and thus an equilibrium constant.

EQUILIBRIUM CONSTANTS

Format

Some of the three-body reactions in Table 2 form products which are thermally unstable at atmospheric temperatures. In such cases the thermal decomposition reaction may compete with other loss processes, such as photodissociation or radical attack. Table 3 lists the equilibrium constants, K(T), for several reactions which may fall into this category. The table has three column entries, the first two being the parameters A and B which can be used to express K(T):

$$K(T)/cm^3\ molecule^{-1} = A\ \exp(B/T)\ (200 < T < 300\ K)$$

The third column entry in Table 3 is the calculated value of K at 298 K.

The data sources for K(T) are described in the individual notes to Table 3.

Definitions

When values of the heats of formation and entropies of all species are known at the temperature T, we note that:

$$\log_{10}[K(T)/cm^3\,molecule^{-1}] = \frac{\Delta S_T^o}{2.303R} - \frac{\Delta H_T^o}{2.303RT} + \log_{10}(T) - 21.87$$

Where the superscript "o" refers to a standard state of one atmosphere. In some cases K values were calculated from this equation, using thermochemical data. In other cases the K values were calculated directly from kinetic data for the forward and reverse reactions. When available, JANAF values were used for the equilibrium constants. The following equations were then used to calculate the parameters A and B:

$$B/^oK = 2.303\log_{10}(K_{200}/K_{300})\left[(300\cdot 200)/(300-200)\right]$$
$$= 1382\log_{10}(K_{200}/K_{300})$$

$$\log_{10} A = \log_{10} K(T) - B/(2.303T)$$

The relationships between the parameters A and B and the quantities $\Delta S^o(298K)$ and $\Delta H^o(298K)$ are as follows:

$$A = (eR'T/N_{av})\exp(\Delta S^o/R) = 3.7 \times 10^{-22}\ T\ \exp(\Delta S^o/R)$$

$$B = -\Delta H^o/R - T(K)$$

Table 3: Equilibrium Constants
(Shaded areas indicate changes or additions since the last version)

Reaction	A/cm^3 molecule^{-1}	B±ΔB/°K	K_{eq}(298 K)	f(298 K)[a]	Note
$NO_2 + NO_3 \rightarrow N_2O_5$	3.0×10^{-27}	10991±200	3.1×10^{-11}	1.2	4
$ClO + ClO \rightarrow ClOOCl$	1.27×10^{-27}	8744±500	7.0×10^{-15}	1.3	11

K/cm^3 molecule^{-1} = A exp (B/T) [200 < T/K < 300]

a f(298) is the uncertainty factor at 298 K. To calculate the uncertainty at other temperatures, use the expression:

$$f(T) = f(298\ K) \exp\left[\Delta B \left(\frac{1}{T} - \frac{1}{298} \right) \right].$$

Notes to Table 3

4. **$NO_2 + NO_3$**. The recommendation is from Pritchard [254] who computed the entropy as a function of temperature and suggested a "Third Law" expression. Pritchard [254] examined the data of Cantrell et al. [54], Burrows et al. [47], Graham and Johnston [118], Wangberg et al [339], Schott and Davidson [281], and the room temperature data of Tuazon et al. [326], Perner et al. [249] and Hjorth et al. [147]. He also included the values given by Smith et al. [295], and Kircher et al. [179], who combined data on the forward reaction, tabulated in Table 2, with decomposition data of by Connell and Johnston [69] and Viggiano et al. [331]. The recommended value is in excellent agreement with the results of Cantrell et al. [56], who report rate constants for the decomposition reaction, which they combine with the rate constants of Orlando et al. [243] to obtain the equilibrium constant. Wangberg et al. [338] measured the equilibrium constant between 280 and 294K and report results in agreement with this recommendation.

11. **ClO + ClO**. The value is from a third-law calculation based on the data from Cox and Hayman [73] (except for their lowest two points) and Nickolaisen et al. [234]. The entropy of ClOOCl, the value of which is 72.2 cal mol^{-1} K^{-1} at 300K, is calculated from structural and spectroscopic data given by Birk et al. [31]. The heat of formation at 300K is $\Delta H^0_{f,300}$ = 30.8 kcal mol^{-1}. A study of branching ratios of ClO + ClO channels in $Cl_2/O_2/O_3$ mixtures by Horowitz et al.[150] also finds the equilibrium constant in O_2 at 285 K to be in agreement with the recommendation. The error limits are chosen to encompass the data.

PHOTOCHEMICAL DATA

The photochemical reactions considered in the current evaluation are the following:

$$O_3 + h\nu \rightarrow O(^1D) + O_2$$
$$ClOOCl + h\nu \rightarrow \text{ products}$$
$$HOCl + h\nu \rightarrow \text{products}$$
$$HOBr + h\nu \rightarrow \text{products}$$

Discussion of Format and Error Estimates

Recommended reliability factors for some of the more important photochemical reactions are given in the Notes. These factors represent the combined uncertainty in cross sections and quantum yields, taking into consideration the atmospherically important wavelength regions, and they refer to the total dissociation rate regardless of product identity.

The error estimates are not rigorous numbers resulting from a detailed error propagation analysis of statistical manipulations of the different sets of literature values; they merely represent a consensus among the panel members as to the reliability of the data for atmospheric photodissociation calculations, taking into account the difficulty of the measurements, the agreement among the results reported by various groups, etc.

The absorption cross sections are defined by the following expression of Beer's Law:

$$I = I_o \exp(-\sigma n l),$$

where Io and I are the incident and transmitted light intensity, respectively; σ is the absorption cross section in cm^2 $molecule^{-1}$; n is the concentration in molecule cm^{-3}; and l is the pathlength in cm. The cross sections are room temperature values at the specific wavelengths listed in the table, and the expected photodissociation quantum yields are unity, unless otherwise stated.

$O_3 + h\nu \rightarrow O + O_2$

Quantum yield for production of $O(^1D)$

In the past few years, the quantum yields for the production of $O(^1D)$ in the photolysis of O_3 in the wavelength range $290 < \lambda < 330$ nm have been measured using sensitive and selective methods at 298 K and below [10,14-17,290,309-311,313,314]. The first finding of these studies is that $O(^1D)$ is produced in ozone photolysis at wavelengths longer than 310 nm, which is the threshold for $O(^1D)$ production in photolysis of ground vibrational levels of ozone assuming spin conservation (i.e., the only co-product of $O(^1D)$ is $O_2(^1\Delta)$). This $O(^1D)$ production at wavelengths longer than 310 nm leads to the existence of the "tail." The tail is now known to be due to two processes: (1) a spin-disallowed channel where $O(^1D)$ and $O_2(^3\Sigma)$ are produced and (2) the photolysis of vibrationally excited ozone. The contribution of vibrationally excited ozone decreases with decreasing temperature such that it is essentially zero by 200 K. These recent studies have substantially improved our knowledge on the existence of the tail reported in some earlier studies[11,35,36,325].

The quantum yield in the wavelength range of 248 to 300 nm is recommended to be 0.95, independent of temperature, with an uncertainty of ±5% (1σ). The recommendation for the wavelength range of 300 to 345 nm is based on the data of Ball et al.[15], Silvente et al.[290], Armerding et al.[10], Trolier and Wiesenfeld.[325], Brock and Watson[35,36], Talukdar et al.[313,314], and Takahashi et al.[309-311] at 298 K. The temperature dependence of the variation of the quantum yield with wavelength is based on the data of Talukdar et al. [314] and Takahashi et al [310,311]. The equation used to fit these data between 300 and 340 nm is given below and it attempts to capture the existence of the two unusual $O(^1D)$ production processes discussed above, along with the spin-allowed channel above ~310 nm.

To obtain the recommended values given below, all the 298 K data between 300 and 340 nm noted above were first fitted to an equation containing 3 Gaussian functions and a constant term, using a non-linear least squares method. The highly wavelength resolved data of Takahashi et al. was binned into 1-nm intervals in this fit. Then, the fit for 298 K was used with the temperature dependence data of Talukdar and Takahashi et al. (again binned into 1 nm intervals) to derive the equation for the temperature dependence that is listed below. In this fitting, the greater-than-unity quantum yields reported by Silvente et al. around 310 nm were excluded. Also, we did not change any of the normalizations made in individual studies for pinning the quantum yields to a specific value at a specific wavelength.

$$\Phi(T,\lambda) = a_1 \exp\left[-\left\{\frac{(\lambda-\lambda_{01})}{\omega_1}\right\}^4\right] + a_2\left(\frac{T}{300}\right)^4 \exp\left(-\frac{\nu_2}{kT}\right)\exp\left[-\left\{\frac{(\lambda-\lambda_{02})}{\omega_2}\right\}^2\right]$$

$$+a_3 \exp\left(-\frac{\nu_3}{kT}\right)\exp\left[-\left\{\frac{(\lambda-\lambda_{03})}{\omega_3}\right\}^2\right] + 0.06$$

In this equation, λ is in nm, T in K, and kT is in wavenumbers (i.e., $k = 0.695\ cm^{-1}\ K^{-1}$).
This parameterization is valid only for the range $300 \le \lambda \le 330$ nm.

Table 4 lists the parameters for the O_3 quantum yield equation.

Table 4: Parameters for the O_3 Quantum Yield Equation

Index	a_i	λ_{oi}	v_i	ω_i
1	0.887	302		7.9
2	2.35	311.1	820	2.2
3	57	313.9	1190	7.4

For $240 < \lambda < 300$ nm, we recommend a wavelength and temperature independent value of 0.95. This assumption of constant quantum yield does not significantly alter the calculated $O(^1D)$ production rates in the atmosphere. However, it could lead to errors in laboratory studies. Thus, for laboratory studies, original literature should be consulted.

There is some evidence for a finite $O(^1D)$ quantum yield at $\lambda > 340$ nm. We are recommending a constant temperature independent value of 0.06 for 330 to 345 nm. However, the uncertainty in the quantum yields at $\lambda > 330$ nm are much larger than for those below 330 nm. This constant value of 0.06 is for atmospheric calculations only. Laboratory studies should not rely on this value for wavelength between 330 and 345 nm.

The uncertainty in the quantum yields between 248 and 300 nm is estimated to be ±5% (1σ). Between 300 and 320 nm, the uncertainty is estimated to be ±20% (1 σ) at temperatures between 200 and 300 K. Between 320 and 340 nm, the uncertainty is estimated to be ±25% (1 σ) at temperatures between 200 and 300 K.

Figure 2 shows the recommended quantum yield for the formation of $O(^1D)$ from the photodissociation of ozone in the 300-340 nm spectral region over the temperature range 200-300 K. The curves are from the empirical expression in the Note.

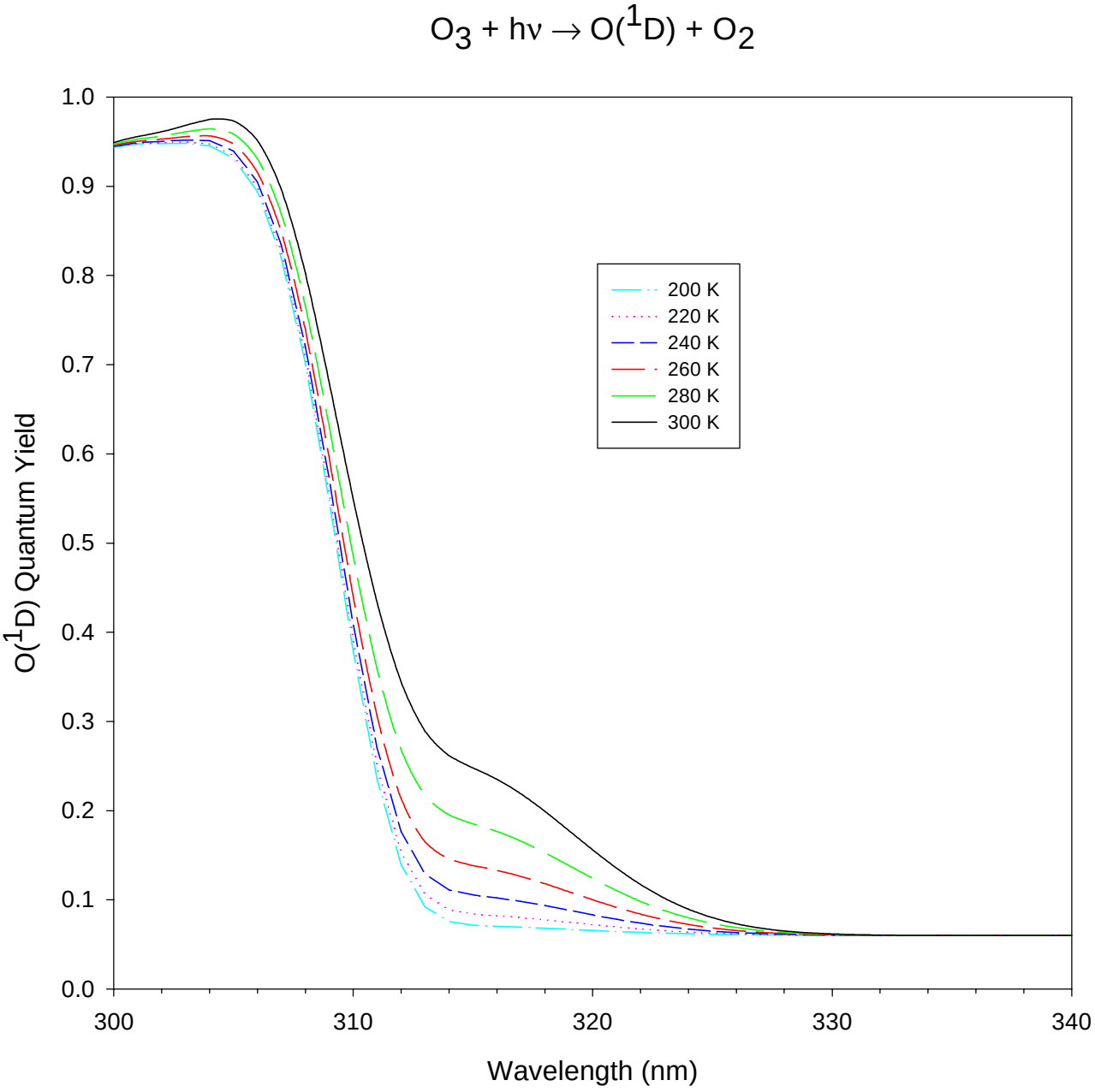

Figure 2: Recommended Photolysis Quantum Yield for the Formation of $O(^1D)$ from O_3.

$ClOOCl + h\upsilon \rightarrow Cl + ClOO$

Recommended absorption cross sections in the wavelength range 190-450 nm for ClOOCl are listed in Table 30 of JPL 97-4 [92]. The values for the wavelength range 200 - 360 nm are the average of experimental results reported by Cox and Hayman [73], DeMore and Tschuikow-Roux [94], Permien et al. [248], and Burkholder et al. [43]. For the 190 - 200 nm range the data are from DeMore and Tschuikow-Roux [94], these being the only data available in that range. Data at wavelengths greater than 360 nm were obtained from a linear extrapolation of the logarithm of the cross sections, using the expression $\log[10^{20}\ \sigma\ (cm^2)] = -0.01915 \times \lambda(nm) + 7.589$. For $\lambda > 360$ nm the extrapolated data are considered to be more reliable than the experimental measurements because of the very small dimer cross sections in this region.

While the results of Cox and Hayman, DeMore and Tschuikow-Roux, Permien et al., and Burkholder et al. are in good agreement at wavelengths below 250 nm, there are significant discrepancies at longer wavelengths, which may be attributed to uncertainties in the spectral subtraction of impurities such as Cl_2O, Cl_2 and Cl_2O_2. Huder and DeMore [154] measured ClOOCl cross sections over the 190 - 310 nm range using a method that minimized the corrections required for impurities such as Cl_2O. The cross sections from this study are significantly smaller (up to a factor of 2) than the current recommendation, particularly when extrapolated beyond 400 nm. Additional measurements are needed, particularly at the longer wavelengths, to check the results of Huder and DeMore.

These studies also indicate that only one stable species is produced in the recombination reaction of ClO with itself, and that this species is dichlorine peroxide, ClOOCl, rather than ClOClO. Using submillimeter wave spectroscopy, Birk et al. [31] have further established the structure of the recombination product to be ClOOCl. These observations are in agreement with the results of quantum mechanical calculations (McGrath et al. [214,215]; Jensen and Odershede [162]; Stanton et al. [305]).

The experiments of Cox and Hayman [73] indicate that the main photodissociation products at 253.7 nm are Cl and ClOO. Molina et al. [222] measured the quantum yield ϕ for this channel to be unity at 308 nm, with no ClO detectable as a product, with an experimental uncertainty in ϕ of about ± 25%. Moore et al. [230] measured the quantum yield for the Cl + ClOO channel at 248 and 308 nm to be 0.9 ± 0.1 and 0.1 ± 0.1 for the 2 ClO channel, and thus supported the study of Molina et al. [222]. These results are also supported by quantum mechanical calculations (Stanton et al. [305]; Stanton and Bartlett [304]). In contrast, Eberstein [103] suggested a quantum yield of unity for the production of two ClO radicals, based merely on an analogy with the photolysis of H_2O_2 at shorter wavelengths. For atmospheric photodissociation calculations the recommended quantum yield value is based on the work of Molina et al. [222] and Moore et al. [230], i.e., a quantum yield $\phi \geq 0.90$ for the Cl + ClOO channel.

$HOCl + h\upsilon \rightarrow OH + Cl$

The absorption cross sections of HOCl vapor have been measured by several groups. Molina and Molina [221] and Knauth et al. [182] produced this species using equilibrium mixtures with Cl_2O and H_2O; their results provided the basis for the earlier recommendation. More recently, Mishalanie et al. [220] and Permien et al. [248] used a dynamic source to generate the HOCl vapor. The cross section values reported by Molina and Molina [221], Mishalanie et al. [220], and Permien et al. [248] are in reasonable agreement between 250 and 330 nm. In this wavelength range, the values reported by Knauth et al. [182] are significantly smaller, e.g., a factor of 4 at 280 nm. Beyond 340 nm, the cross sections of Mishalanie et al. are much smaller than those obtained by the other three groups. At 365 nm, the discrepancy is about an order of magnitude.

Burkholder [40] has remeasured the absorption spectrum of HOCl over the wavelength range 200 to 380 nm, following photolysis of equilibrium mixtures of Cl_2O-H_2O-HOCl. The obtained spectrum displays two absorption maxima at 242 and 304 nm, and is in excellent agreement with the work of Knauth et al. [182], but in poor agreement with the measurements of Mishalanie et al. [220] and Permien et al. [248]. The discrepancies can be attributed mostly to difficulties in correcting the measured absorptions for the presence of Cl_2 and Cl_2O. In the study by Burkholder, several control experiments were carried out in order to check the internal consistency of the data. Moreover, Barnes et al. [19] examined the near-UV spectrum of HOCl by monitoring the OH fragments resulting from photodissociation, and revealed a third weak band centered at 387 nm extending down to 480 nm. The recommended cross sections up to 420 nm, calculated from an analytical expression provided by Barnes et al. [19] and based on the values of Burkholder [40] and Barnes et al. [19], are listed in Table 5. The work by Jungkamp et al. [165] yields cross section values in excellent agreement with this recommendation for wavelengths shorter than 350 nm.

Molina et al. [223] observed production of OH radicals in the laser photolysis of HOCl around 310 nm, and Butler and Phillips [51] found no evidence for O-atom production at 308 nm, placing an upper limit of ~0.02 for the primary quantum yield for the HCl + O channel. Vogt and Schindler [332] used broadband photolysis in the 290 - 390 nm wavelength range, determining a quantum yield for OH production of >0.95.

Table 5: Absorption Cross Sections of HOCl
(Shaded areas indicate changes or additions since the last version)

λ (nm)	10^{20} σ (cm^2)	λ (nm)	10^{20} σ (cm^2)	λ (nm)	10^{20} σ (cm^2)
200	7.18	274	5.26	348	1.55
202	6.39	276	4.94	350	1.43
204	5.81	278	4.74	352	1.33
206	5.46	280	4.64	354	1.24
208	5.37	282	4.62	356	1.17
210	5.54	284	4.68	358	1.11
212	5.98	286	4.79	360	1.06
214	6.68	288	4.95	362	1.02
216	7.63	290	5.13	364	0.985
218	8.81	292	5.33	366	0.951
220	10.2	294	5.52	368	0.919
222	11.6	296	5.71	370	0.888
224	13.2	298	5.86	372	0.855
226	14.7	300	5.99	374	0.822
228	16.2	302	6.08	376	0.786
230	17.5	304	6.12	378	0.748
232	18.7	306	6.12	380	0.708
234	19.6	308	6.07	382	0.667
236	20.2	310	5.97	384	0.624
238	20.5	312	5.84	386	0.580
240	20.6	314	5.66	388	0.535
242	20.3	316	5.45	390	0.491
244	19.8	318	5.21	392	0.447
246	19.0	320	4.95	394	0.405
248	18.1	322	4.67	396	0.364
250	17.0	324	4.38	398	0.325
252	15.8	326	4.09	400	0.288
254	14.6	328	3.79	402	0.254
256	13.3	330	3.50	404	0.222
258	12.1	332	3.21	406	0.194
260	10.9	334	2.94	406	0.168
262	9.73	336	2.68	410	0.144
264	8.68	338	2.44	412	0.124
266	7.75	340	2.22	414	0.105
268	6.94	342	2.02	416	0.089
270	6.25	344	1.84	418	0.075
272	5.69	346	1.69	420	0.063

HOBr + hυ → Products

The absorption spectrum of HOBr has been measured by Orlando and Burkholder [241], Deters et al. [95], Benter et al. [29], Rattigan et al. [259], and Ingham et al. [159]. The spectra cluster in two groups. Orlando and Burkholder [241], Deters et al. [95], and Benter et al. [29] observe between 240 and 400 nm two absorption bands with maxima near 284 and 351 nm; the spectra agree reasonably well in their shape, but show a sharp decrease in cross section above 400 nm. In contrast, the cross sections reported by Rattigan et al. [259] and Ingham et al. [159] are roughly 50 % larger between 300 and 400 nm.

In addition, the spectrum obtained by Rattigan et al. shows a pronounced tail extending to 520 nm, whereas Ingham et al. observe unambiguously a third weaker absorption band ranging to 550 nm with a maximum at 457 nm. These last two studies confirm the observations of Barnes et al. [18], who showed that laser photolysis of HOBr between 440-600 nm gives rise to OH fragments. The presence of a weak band beyond 400 nm is attributable to the presence of a forbidden transition from the ground electronic to a triplet state predicted by the ab initio calculations of Francisco et al. [110]. The differences in the spectral shapes are probably attributable to impurities such as Br_2O and Br_2, and/or the use of different Br_2O cross sections. However, the presence of impurities alone cannot explain the large difference in cross sections at the peak of the absorption bands.

The recommended absorption cross sections are listed in Table 6, in the range from 250 to 550 nm; below 250 nm the data are uncertain and no recommendation is given. The cross section values in the table are based on the latest study by Ingham et al. [159]. These authors generated HOBr in situ by laser photolytic production of OH in the presence of Br_2, and determined the HOBr spectrum using a gated diode camera shortly after the pulse, circumventing the problem associated with the presence of the strong absorbing impurity Br_2O, which was encountered in previous studies. The calibration of the absorption cross sections was made relative to the established cross sections of Br_2.

The data presented in Table 6 are computed with the following expression taken from Ingham et al. [159], which is based on a combination of three Gaussian fits, one for each absorption band:

$$\sigma(\lambda) = 24.77\exp\left\{-109.80\left[\ln\left(\frac{284.01}{\lambda}\right)\right]^2\right\} + 12.22\exp\left\{-93.63\left[\ln\left(\frac{350.57}{\lambda}\right)\right]^2\right\} + 2.283\exp\left\{-242.40\left[\ln\left(\frac{457.38}{\lambda}\right)\right]^2\right\}$$

$\sigma(\lambda)$: 10^{-20} cm^2 molecule^{-1}; $250 < \lambda < 550$ nm.

Benter et al. [29] measured quantum yields for HOBr photolysis at 261 and 363 nm (near the peaks of the second absorption bands). The observed quantum yield for Br formation at 363 nm was greater than 0.95, and an unity quantum yield into the product channel OH + Br is recommended. The other channel O + HBr was not observed. The laser photofragment study of Barnes et al. [18] claimed that OH was the major photolysis product at wavelengths beyond 400 nm. Lock et al. [207] found that at 490 and 510 nm OH and Br fragments are in their respective vibrational and spin-orbit ground states. The assumption of unit quantum yield of OH formation should be confirmed experimentally.

Table 6: Absorption Cross Sections of HOBr

(Shaded areas indicate changes or additions since the last version)

λ (nm)	10^{20} σ (cm^2)	λ (nm)	10^{20} σ (cm^2)	λ (nm)	10^{20} σ (cm^2)
250	4.15	355	12.1	460	2.28
255	6.19	360	11.5	465	2.14
260	10.5	365	10.5	470	1.91
265	14.6	370	9.32	475	1.62
270	18.7	375	7.99	480	1.30
275	22.1	380	6.65	485	0.993
280	24.3	385	5.38	490	0.723
285	25.0	390	4.22	495	0.502
290	24.0	395	3.23	500	0.333
295	21.9	400	2.43	505	0.212
300	19.1	405	1.80	510	0.129
305	16.2	410	1.36	515	0.076
310	13.6	415	1.08	520	0.042
315	11.8	420	0.967	525	0.023
320	10.8	425	0.998	530	0.012
325	10.5	430	1.15	535	0.0059
330	10.8	435	1.40	540	0.0029
335	11.3	440	1.68	545	0.0013
340	11.9	445	1.96	550	0.0006
345	12.3	450	2.18		
350	12.4	455	2.29		

HETEROGENEOUS CHEMISTRY

We have evaluated and tabulated the currently available information on heterogeneous stratospheric processes. In addition, because of the increasing level of interest in tropospheric processes with a direct bearing on the fluxes of reactive species into the stratosphere, such as heterogeneous loss processes for partially oxidized degradation products of hydrohalocarbons and heterogeneous contrail and cloud processing of exhaust species from aircraft, we have included kinetic data for selected heterogeneous interactions relevant to modeling cloud droplet and aqueous aerosol chemistry in the free troposphere.

However, both stratospheric and tropospheric heterogeneous chemistry are relatively new and rapidly developing fields, and further results can be expected to change our quantitative and even our qualitative understanding on a regular basis. The complexity is compounded by the difficulty of characterizing the chemical and physical properties of atmospheric heterogeneous surfaces and then reproducing suitable simulations in the laboratory [185].

Surface Types

To a first approximation there are three major types of surfaces believed to be present at significant levels in the stratosphere. They are: 1) Type I - polar stratospheric clouds (PSCs), nominally composed of nitric acid trihydrate ($HNO_3 \cdot 3H_2O$); 2) crystals of relatively pure water ice, designated as Type II PSCs because they form at lower temperatures than Type I and are believed to be nucleated by Type I (similar surfaces may form as contrails behind high-altitude aircraft under some stratospheric conditions); and 3) sulfuric acid aerosol, which is nominally a liquid phase surface generally composed of 60 - 80 weight percent H_2SO_4 and, concomitantly, 40-20 weight percent H_2O.

While PSCs, as their name suggests, are formed primarily in the cold winter stratosphere at high latitudes, sulfuric acid aerosol is present year round at all latitudes and may influence stratospheric chemistry on a global basis, particularly after large injections of volcanic sulfur episodically increase their abundance and surface area. There is also increasing evidence that ternary $H_2SO_4/HNO_3/H_2O$ liquid solutions may play a significant role in PSC formation.

In addition to the major stratospheric surface types noted above, several other types of heterogeneous surfaces are found in the stratosphere and may play a significant role in some stratospheric processes. For instance, recent laboratory work has indicated that nitric acid dihydrate (NAD) may play an important role in the nucleation of Type I PSCs (Worsnop et al. [348]; Fox et al. [109]) and that mixtures of solid nitric acid hydrates and sulfuric acid tetrahydrate (SAT) (Molina et al. [227]; Zhang et al. [360]) and/or a more complex sulfuric acid/nitric acid hydrate (Fox et al. [109]) may also be key to understanding Type I PSC nucleation and evolution.

Analyses of the range of atmospheric conditions possible in the polar stratosphere have also led to interest in solid SAT surfaces and possibly other forms of frozen sulfuric acid aerosols (Toon et al. [322]; Middlebrook et al. [219]), as well as liquid sulfuric acid aerosols significantly more dilute than the 60-80 weight percent normally present at lower latitudes (Wolff and Mulvaney [347]; Hofmann and Oltmans [149]; Toon et al. [322]).

Some modeling studies also suggest that certain types of major volcanic eruptions transport significant levels of sodium chloride into the stratosphere (Michelangeli et al. [218]), so studies of stratospheric trace species interacting with solid NaCl or similar salts, as well as salt solutions, have also been included.

Finally, aircraft and rocket exhausts contribute small but measurable amounts of carbonaceous soot (Pueschel et al. [257]) and aluminized solid propellant rocket exhausts and spacecraft debris produce increasing levels of alumina (Al_2O_3) and similar metal oxide particles (Zolensky et al. [361]) in the stratosphere. In the free troposphere the primary heterogeneous surfaces of interest are liquid or solid water (cloud droplets, contrails) or aqueous sulfate solutions representative of background aerosols.

The detailed composition and morphology of each surface type are uncertain and probably subject to a significant range of natural variability. Certain chemical and physical properties of these surfaces, such as their ability to absorb and/or solvate HCl and HNO_3, are known to be strongly dependent on their detailed chemical composition. Moreover, most heterogeneous processes studied under laboratory conditions (and in some cases proceeding under stratospheric conditions) can change the chemical composition of the surface in ways that significantly affect the kinetic or thermodynamic processes of interest.

Thus, a careful analysis of the time-dependent nature of the active surface is required in the evaluation of measured uptake kinetics experiments. Experimental techniques which allow the measurement of mass accommodation or surface reaction kinetics with high time resolution and/or with low trace gas fluxes are often more credible in establishing that measured kinetic parameters are not seriously compromised by surface saturation or changing surface chemical composition.

The measured kinetic uptake parameters, mass accommodation coefficients, and surface reaction probabilities are separately documented for relevant atmospheric trace gas species for the major and, where available, the minor stratospheric surfaces noted above.

Since these parameters can vary significantly with surface composition (e.g., the H_2SO_4/H_2O ratio for sulfate aerosol or the HNO_3/H_2O ratio for Type I PSC) the dependence of these parameters on surface composition is reviewed where sufficient data are available. Furthermore, data are also compiled for liquid water for several reasons.

First, this surface is one asymptote of the H_2SO_4/H_2O aerosol continuum; second, the interactions of some trace species with liquid water and water ice (Type II PSC) surfaces are often similar; and third, the uptake of some trace species by water surfaces in the troposphere can play a key role in understanding their tropospheric chemical lifetimes and, thus, the fraction that may be transported into the stratosphere.

Surface Porosity

The experimental techniques utilized to measure mass accommodation, heterogeneous reaction, and other uptake coefficients generally require knowledge of the surface area under study. For solid surfaces, and most particularly for water and acid ice surfaces formed in situ, the determination of how the molecular scale ice surface differs from the geometrical surface of the supporting substrate is not easy.

Keyser, Leu, and coworkers have investigated the structure of water and nitric acid ice films prepared under conditions similar to those used in their flow reactor for uptake studies (Keyser et al. [178]; Keyser and Leu [176]; Keyser and Leu [175]). They have demonstrated that ice films grown in situ from the vapor can have a considerably larger available surface than that represented by the geometry of the substrate; they have also developed a simple model to attempt to correct measured uptake rates for this effect (Keyser et al. [178]; Keyser et al. [177]).

This model predicts that correction factors are largest for small uptake coefficients and thick films.

The application of the model to experimental uptake data remains controversial (Keyser et al. [177]; Hanson and Ravishakara [133]; Kolb et al. [185]). Some experimenters prefer to attempt growing ice surfaces as smooth as possible and to demonstrate that their measured uptake coefficients are only weakly dependent on surface thickness (Hanson and Ravishankara, [132]).

Similar issues arise for uptake experiments performed on powered, fused and single crystal salt or oxide surfaces (Fenter et al.[106]; Hanning-Lee et al. [123]). The degree to which measured uptake parameters must be corrected for porosity effects will remain in some doubt until a method is devised for accurately determining the effective surface area for the surfaces actually used in uptake studies. Most studies evaluated in this review assume that the effective ice or salt surface area is the geometrical area.

Temperature Dependence

A number of laboratory studies have shown that mass accommodation coefficients and, to some extent, surface reaction probabilities can be temperature dependent. While these dependencies have not been characterized for many systems of interest, temperature effects on kinetic data are noted where available. More work that fully separates heterogeneous kinetic temperature effects from temperature controlled surface composition is obviously needed.

Solubility Limitations

Experimental data on the uptake of some trace gases by various stratospherically relevant surfaces can be shown to be governed by solubility limitations rather than kinetic processes. In these cases properly analyzed data can yield measurements of trace gas solubility parameters relevant to stratospheric conditions.

In general, such parameters can be strongly dependent on both condensed phase composition and temperature. Such parameters may be very important in stratospheric models, since they can govern the availability of a reactant for a bimolecular heterogeneous process (e.g., the concentration of HCl available for the HCl + $ClONO_2$ reaction on sulfuric acid aerosols) or the gas/condensed phase partitioning of a heterogeneous reaction product (e.g., the HNO_3 formed by the reaction of N_2O_5 on sulfuric acid aerosols).

Data Organization

Data for selected trace gas surface reaction probabilities with relevant condensed phase surfaces are tabulated in Table 7. Evaluated data for mass accommodation coefficients and solubilities are given in Tables 63 and 65 of DeMore et al. [92].

Parameter Definitions

Mass accommodation coefficients (α), represent the probability of reversible uptake of a gaseous species colliding with the condensed surface of interest. For liquid surfaces this process is associated with interfacial (gas-to-liquid) transport and is generally followed by bulk liquid phase solvation. Examples include: simple surface absorption, absorption followed by ionic dissociation and solvation (e.g., $HCl + nH_2O \leftrightarrow H^+(aq) + Cl^-(aq)$), and absorption followed by a reversible chemical reaction with a condensed phase substituent (e.g., $SO_2 + H_2O \leftrightarrow H^+ + HSO_3^-$ or $CH_2O + H_2O \leftrightarrow CH_2(OH)_2$).

The term "sticking coefficient" is often used for mass accommodation on solid surfaces where physisorption or chemisorption takes the place of true interfacial mass transport.

Processes involving liquid surfaces are subject to Henry's law, which limits the fractional uptake of a gas phase species into a liquid. If the gas phase species is simply solvated, a physical Henry's law constraint holds; if the gas phase species reacts with a condensed phase substituent, as in the sulfur dioxide or formaldehyde hydrolysis cases noted above, a "chemically modified" or "effective" Henry's law constraint holds (Clegg and Brimblecombe [62]; Schwartz [285]; Watson et al. [341]). Henry's law constants relate the equilibrium concentration of a species in the gas phase to the concentration of the same species in a liquid phase, and they have, in this report, units of $M\ atm^{-1}$.

Effective Henry's law constants are designated H*, while simple physical Henry's law constants are represented by H. Effective Henry's law constants are also employed to represent decreased trace gas solubilities in moderate ionic strength acid or salt solutions with the use of a Setchenow coefficient formulation which relates H* to the concentration of the acid or salt [158]. It is presently unclear whether "surface solubility" effects govern the uptake on nominally solid water ice or HNO_3/H_2O ice surfaces in a manner analogous to bulk solubility effects for liquid substrates.

For some trace species on some surfaces, experimental data suggest that mass accommodation coefficients untainted by experimental saturation limitations have been obtained. In other cases experimental data can be shown to be subject to Henry's law constraints, and Henry's law constants, or at least their upper limits, can be determined. Some experimental data sets are insufficient to determine if measured "uptake" coefficients are true accommodation coefficients or if the measurement values are lower limits compromised by saturation effects.

Surface reaction probabilities (γ) are kinetic values for generally irreversible reactive uptake of trace gas species on condensed surfaces. Such processes may not be rate limited by Henry's law constraints; however, the fate of the uptake reaction products may be subject to saturation limitations. For example, N_2O_5 has been shown to react with sulfuric acid aerosol surfaces. However, if the H_2SO_4/H_2O ratio is too high, the product HNO_3 will be insoluble, and a large fraction will be expelled back into the gas phase. Surface reaction probabilities for substantially irreversible processes are presented in Table 7. Reaction products are identified where known.

The total experimental uptake coefficient measured in laboratory heterogeneous kinetic experiments are also often symbolized by the symbol γ. In those cases where surface and/or bulk reaction dominate the uptake, the total uptake coefficient (γ_{total}) and reactive uptake coefficient (γ_{total}) may well be identical. More formally, for cases where bulk liquid phase reaction is facile

and there are no gas phase diffusion constraints, the total uptake coefficient can be approximated in terms of γ_{rxn} and γ_{sol} as [185]:

$$\frac{1}{\gamma_{total}} = \frac{1}{\alpha} + \frac{1}{\gamma_{sol} + \gamma_{rxn}}$$

where

$$\gamma_{sol} = \frac{4HRT}{\pi^{1/2}\,\bar{c}} \left(\frac{D}{t}\right)^{1/2}$$

and

$$\gamma_{rxn} = \frac{4HRT}{\bar{c}} \left(Dk_{rxn}\right)^{1/2}$$

where t is the time the trace gas is exposed to the liquid surface, R is the gas constant, D is the liquid phase diffusion coefficient, and $\bar{c}$ is the mean trace gas molecular speed. In the limit of low solubility or long exposure time γ_{sol} becomes negligible and:

$$\frac{1}{\gamma_{total}} = \frac{1}{\alpha} + \frac{1}{\gamma_{rxn}} \quad .$$

Discussion of how to use this approach to model chemical reactions in liquid stratospheric aerosols can be found in Hanson et al. [138] and Kolb et al. [185]. Note that these formulations are approximate. In cases where separate terms are competitive, more rigorous solution of kinetic differential operations may be appropriate.

For solid surfaces, bulk diffusion is generally too slow to allow bulk solubility or bulk kinetic processes to dominate uptake. For solids, reactive uptake is driven by chemisorption/chemical reaction at the interface, a process that can also influence trace gas uptake on liquids. In these cases surface reaction (γ_{surf}) occurs in parallel, rather than in series with mass accommodation, thus:

$$\gamma_{total} = \gamma_{surf} + \left[\frac{1}{\alpha} + \frac{1}{\gamma_{sol} + \gamma_{rxn}}\right]^{-1}$$

Examples where this more complex situation holds for liquid surfaces can be found in Hu et al. [153] and Jayne et al.[161]. In such cases γ may be significantly larger than α.

The data in Table 7 are organized by trace gas species, since some systematic variation may be expected for surface accommodation or reaction as the surface composition and/or phase

is varied. Data presented for one surface may be judged for "reasonableness" by comparing with data for a "similar" surface. In some cases it is not yet clear if surface uptake is truly reversible (accommodation) or irreversibly reactive in nature.

Evaluation Process

Publications presenting experimental kinetic parameters for selected reactions in Table 7 appearing since our last evaluation (DeMore et al. [92]) were identified and evaluated. Laboratories known to be studying these reactions were also contacted and asked to provide available data prior to publication. All available data, from both new and previously identified studies were plotted for each reaction/surface combination, as a function of temperature, acid concentration (for water/acid surfaces), and other pertinent experimental parameters. Data were evaluated for biases reflecting surface and/or bulk saturation effects.

In general, data from experiments using the lowest possible trace gas concentrations and/or providing continuously generated fresh surfaces were found to be less affected by surface and/or bulk saturation, and were retained for rate evaluations. All data were plotted in terms of the reactive uptake coefficient, γ, even in cases were γ can be deconvolved to yield more fundamental parameters such as mass accommodation coefficients, Henry's law constants, liquid phase diffusion coefficients, and liquid phase second order rate constants (see Robinson et al. [272] for examples). Data plots generally incorporated the stated statistical uncertainties reported by the authors of the publications reporting the data.

Data free from obvious experimental biases were then least squares fit with an appropriate function, phenomenologically based, if appropriate, and empirical if not. The standard deviation of the fitting function from the data was then determined to yield an estimate of the statistical uncertainty. Were appropriate, systematic uncertainty estimates were evaluated and added to the statistical uncertainty. The results of these evaluations are summarized in Table 7.

Reactions of N_2O_5, $ClONO_2$, HOCl and $BrONO_2$ on/in sulfuric acid are generally dependent on the species' Henry's law solubility and liquid phase diffusion coefficient in the liquid acid as well as the surface and/or liquid phase reaction rate parameters. All of these processes are generally functions of the acid composition and temperature (Hanson et al. [138], Robinson et al. [272]). Thus, these reactions' reactive uptake coefficients must be represented by a complex phenomenological or empirical model which defy simple entry into Table 7. The notes to Table 7 for these reactions discuss and present the models adopted. However, to aid in visualizing the resulting reactive uptake parameters the results for several reactions have been plotted in Figure 1 as a function of temperature for a background pressure of 50 mbar and background water vapor and HCl mixing ratios of 5 ppm and 2 ppb, respectively.

Figure 3 graphs recommended reactive uptake coefficients as a function of temperature for key stratospheric heterogeneous processes on sulfuric acid aerosols. The calculations assume a total pressure of 50 mbar, H_2O vapor mixing ratio of 5 ppm, and HCl mixing ratio of 2 ppb. For this calculation, the aerosol reacto-diffusive length for each reaction is assumed to be small and $P_{HCl} >> P_{ClONO_2}$.

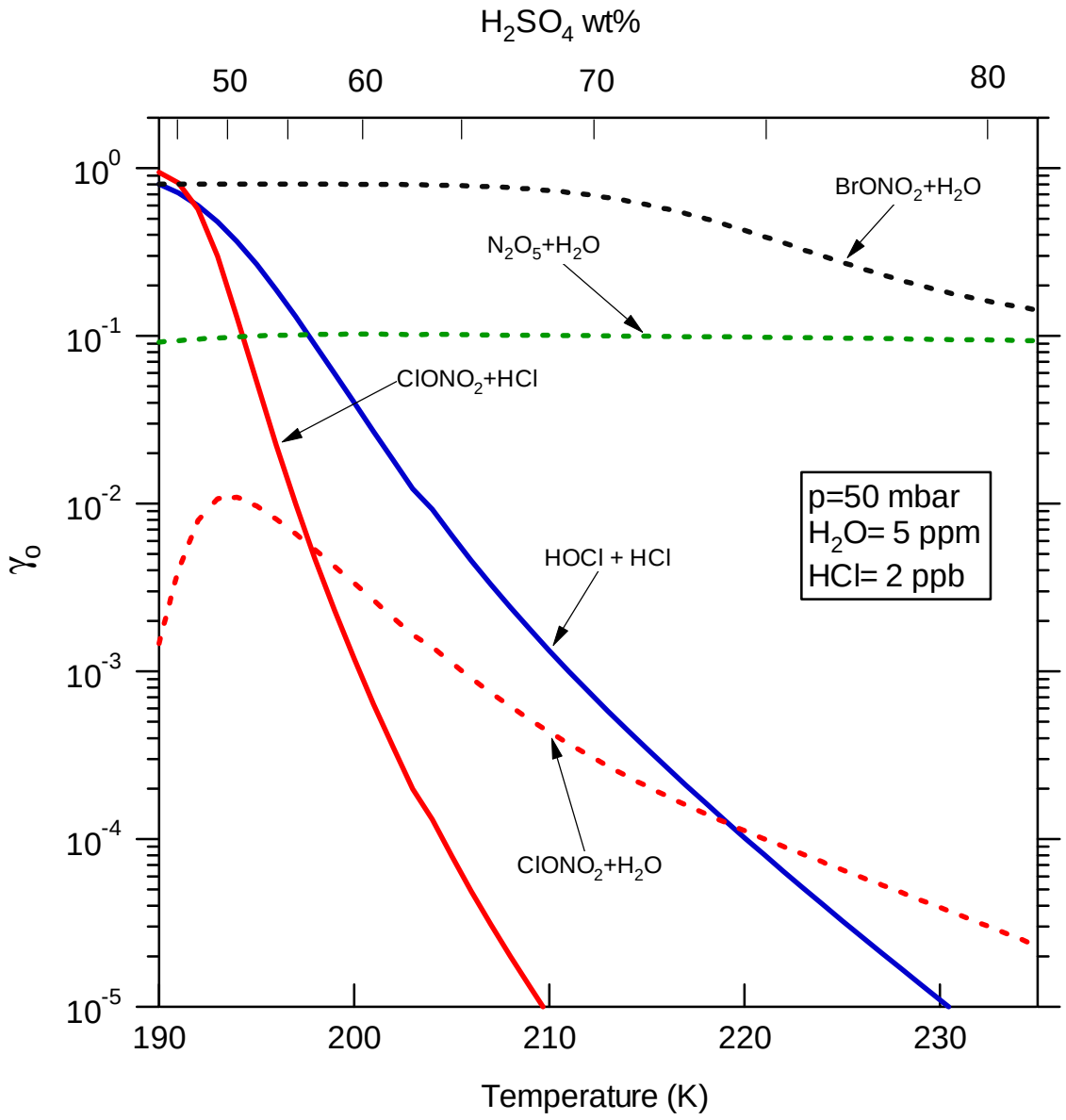

Figure 3: Recommended Reactive Uptake Coefficients as a Function of Temperature for Key Stratospheric Heterogeneous Processes on Sulfuric Acid Aerosols.

Table 7: Gas/Surface Reaction Probabilities (γ)
(Shaded areas indicate changes or additions since the last version)

Gaseous Species	Surface Type	Surface Composition	T(K)	γ	Uncertainty Factor	Notes
$N_2O_5 + H_2O \rightarrow 2HNO_3$						
N_2O_5	Water Ice	H_2O(s)	188-195	0.02	2	14
	Liquid Water	H_2O(l)	260-295	See Note*	See Note	15
	Nitric Acid Ice	$HNO_3 \bullet 3H_2O$(s)	200	4 x 10-4	3	16
	Sulfuric Acid	$H_2SO_4 \bullet nH_2O$(l)	195-300	See Note*	See Note	17
$HOCl + HCl(s) \rightarrow Cl_2 + H_2O$						
HOCl	Water Ice	H_2O(s) • HCl(s)	195-200	0.2	2	40
	Nitric Acid Ice	$HNO_3 \bullet 3H_2O$(s)•HCl(s)	195-200	0.1	2	40
	Sulfuric Acid	$H_2SO_4 \bullet nH_2O$(l)	198-209	See Note*	See Note	41
$ClONO_2 + H_2O(s) \rightarrow HOCl + HNO_3$						
$ClONO_2$	Water Ice	H_2O(s)	180-200	0.3	3	43
	Nitric Acid Ice	$HNO_3 \bullet 3\ H_2O$ (s)	185-202	0.004	3	44
	Sulfuric Acid	$H_2SO_4 \bullet n\ H_2O$ (l)	200-265	See Note*	See Note	45
$ClONO_2 + HCl(s) \rightarrow Cl_2 + HNO_3$						
$ClONO_2$	Water Ice	H_2O(s)	180-200	0.3	3	47
	Nitric Acid Ice	$HNO_3 \bullet 3\ H_2O \bullet HCl$	185-210	0.2	2	48
	Sulfuric Acid	$H_2SO_4 \bullet nH_2O$(l)•HCl(l)	195-235	See Note*	See Note	49
$HOBr + HCl(s) \rightarrow BrCl + H_2O$						
HOBr	Water Ice	H_2O(s) • HBr(s)	228	0.3	3	57
	Sulfuric Acid	$H_2SO_4 \bullet n\ H_2O$ (60-69 wt.% H_2SO_4)	198-218	See Note		57
$BrONO_2 + H_2O \rightarrow HOBr + HNO_3$						
$BrONO_2$	Water Ice	H_2O(s)	190-200	0.3	2	59
	Sulfuric Acid	$H_2SO_4 \bullet nH_2O$	210-300	See Note	See Note	60

*γ is temperature dependent

Notes to Table 7

14. **N_2O_5 + H_2O(s)** - Leu [195] and Hanson and Ravishankara [129] measured nearly identical values of 0.028 (±0.011) and 0.024 (±30%) in the 195-202 K range on relatively thick ice films in coated wall flow tubes. Quinlan et al. [258] measured a maximum value for γ on ice surfaces at 188 K of 0.03 in a Knudsen cell reactor. The average of these three studies is 0.027 with a standard deviation of 0.003. Hanson and Ravishankara [131,132] presented new and re-analyzed data as a function of ice thickness, with a value of ~0.008 for the thinnest ice sample, rising to 0.024 for the thickest. From these data there would appear to be no strong dependence on temperature, at least over the 188-195 K range. It is unclear whether the measured dependence on ice film thickness is due to added porosity surface area in the thicker films or decreased ice film integrity in thinner films. The error estimate in Table 7 is driven by the possible systematic error due to unresolved film thickness effects rather than the small statistical error among the "thick film" values from the three groups.

15. **N_2O_5 + H_2O(l)** - Reaction on liquid water has a negative temperature dependence. Van Doren et al. [328] measured γs of 0.057 ±0.003 at 271 K and 0.036 ±0.004 at 282 K using a droplet train uptake technique. George et al. [115] also used a droplet train technique to measure γs of (3.0 ±0.2) x 10^{-2} (262 K), (2.9 ±1.2) x 10^{-2} (267 K), (2.0 ±0.2) x 10^{-2} (273 K), (1.6 ±0.8) x 10^{-2} (276 K), and (1.3 ±0.8) x 10^{-2} (277 K) on pure water, while Schweitzer et al. [286] used the same approach for pure water and salt solutions between 262 and 278 K, obtaining similar results. Mozurkewich and Calvert [231] studied uptake on $NH_3/H_2SO_4/H_2O$ aerosols in a flow reactor. For their most water-rich aerosols (RH = 76%) they measured γs of 0.10 ±0.02 at 274 and 0.039 ±0.012 at 293 K. However, similar studies by Hu and Abbatt [152] on $(NH_3)_2SO_4$ aerosols at 297 K showed that uptake rises with decreasing relative humidity (RH); their 94% RH results agree very well with the temperature trend measured by Van Doren et al. Msibi et al.[232] measured a smaller γ of 2.5 x 10^{-3} for water adsorbed on a denuder flow tube well under 66-96% relative humidity conditions at room temperature. The higher γ values of Van Doren et al., Mozurkewhich and Calvert, and Hu and Abbatt are quite consistent when temperature and RH effects are factored in. The lower values from the Louis Pasteur (George et al.; Schweitzer et al.) and Birmingham (Msibi et al.) groups appear to have a much less pronounced temperature dependence and are inconsistent with the other measurements. The same function used to fit the N_2O_5 uptake on sulfuric acid as a function of temperature and concentration, discussed in note 17 below, has been extended to the Van Doren et al. and Hu and Abbatt data for pure water and very high RH aerosols. See note 17 for the functional fit and its error discussion.

16. **N_2O_5 + HNO_3•$3H_2O$(s)** - Hanson and Ravishankara [130] have measured γ = 0.0006 (±30%) near 200 K. They presented re-analyzed and additional data as a function of ice thickness (Hanson and Ravishankara [131,132]), deriving a value of 3 x 10^{-4} for the thinnest NAT covered ice layer, with values up to three times higher for thicker NAT-covered ice layers. As in the case of uptake on water ice this may be due to increased surface area from porosity in the thicker films, or less integrity in the thinner films. The uncertainty listed in Table A-1

is driven by this observed effect. All of the Hanson et al. data are in very poor agreement with the $\gamma = 0.015$ (±0.006) reported by Quinlan et al. [258] from their Knudsen cell measurements; this measurement may have been biased by formation of a super-cooled aqueous nitric acid surface and is judged to be unreliable.

17. **N_2O_5 + H_2SO_4•n H_2O (l)** - This reaction has been intensively studied between 195 and 296 K for a wide range of H_2SO_4 wt. % values using four complementary experimental techniques. Data are available from aerosol flow tube studies (Fried et al. [111], Hanson and Lovejoy [126], and Hu and Abbatt [152]), coated wall flow tube studies (Hanson and Ravishankara [129], Zhang et al. [359]), a stirred Knudsen cell (Manion et al. [208]) and droplet train studies (Van Doren et al. [329], Robinson et al. [272]). All studies have yielded γs between ~0.05 and 0.20 with modest dependence on surface H_2SO_4 wt. % and temperature. The Knudsen cell studies, aerosol flow tube studies at higher N_2O_5 exposure and the ternary $H_2SO_4/HNO_3/H_2O$ studies of Zhang et al. all illustrate that significant levels of HNO_3 in the H_2SO_4/ H_2O solutions will reduce γ measurably; this fact explains some of the scatter in aerosol flow tube studies and the surface saturation evident in the Knudsen cell studies. The effects of 5.0×10^{-7} Torr HNO_3 for γ (N_2O_5) as a function of temperature at two water vapor concentrations are plotted in Zhang et al.; the decrease in γ is greatest at low temperatures, approaching a factor of 2-5 between 200 and 195 K.

Experimental data on sulfuric acid surfaces between 40 and 80 wt.% sulfuric acid deemed to be free of saturation effects, plus the pure water uptake data of Van Doren et al. [328] and high relative humidity ammonium sulfate aerosol uptake data of Hu and Abbott [152] were all fit to a polynomial expression to yield a single function describing γ for N_2O_5 uptake valid between 0 and 80 wt.% H_2SO_4 and 180 to 300 K. The form of this function is: $\gamma o = \exp(k_o + k_1/T + k_2/T_2)$, where T is the temperature K. The parameters k_o, k_1, and k_2 obtained from the best-fit are:

$$k_o = -25.5265 - 0.133188wt + 0.00930846wt^2 - 9.0194 \times 10^{-5} wt^3$$

$$k_1 = 9283.76 + 115.345wt - 5.19258wt^2 + 0.0483464wt^3$$

$$k_2 = -851801 - 22191.2wt + 766.916\,wt^2 - 6.85427wt^3$$

where wt is the weight percentage of H_2SO_4.

The overall error of applying the uptake function provided here consists of two components. One is the standard deviation of model-calculated value with respect to measured data, σ_m, which is given by

$$\sigma_m = \sqrt{\frac{\sum_{i=1}^{N} \left(1 - \frac{\gamma_i}{\gamma_{\text{model}}}\right)^2}{N-1}}.$$

The other is the standard deviation of relative experimental measurement error from the mean, σ_d, which is given by

$$\sigma_d = \sqrt{\frac{\sum_{i=1}^{N}\left(\frac{\Delta\gamma_i}{\gamma_{\text{model}}}\right)^2}{N(N-1)}}$$

The overall error is

$$\sigma = \sqrt{\sigma_m^2 + \sigma_d^2}\,.$$

These formulations are also applied below in the error estimation for the $ClONO_2 + H_2O$ and HCl, $BrONO_2 + H_2O$, and HOCl + HCl reactions. For N_2O_5, the error is estimated to be 15% (one sigma), with σ_m=14.7% and σ_d=2.9% .

40. **HOCl + HCl + H_2O(s) and HNO_3•3H_2O(s)** - Hanson and Ravishankara [131] and Abbatt and Molina [5] have investigated the HOCl + HCl reaction on water ice and NAT-like surfaces, and Chu et al. [61] studied the reaction on water ice. Product yield measurements support the identification of Cl_2 and H_2O as the sole products. The measured yield of product Cl_2 is 0.87 ±0.20 and was stated to be similar on both surfaces [Abbatt and Molina]. Within the accuracy of the experiments, the reaction probability does not depend on the gas phase HCl and HOCl densities. Only Abbatt and Molina investigated at more than one temperature, their data indicates that γ increases at lower temperatures. A plot of data from the three studies does show a weak temperature trend, with γ increasing about a factor of two as the temperature drops from 202 to 188 K. However, the data are too sparse to assign a definitive temperature dependence. The average of all three studies yields $\gamma = 0.26 \pm 0.08$ for data based on the geometrical area of the flow tube surfaces. Chu et al. indicate that a porosity correction for their data would reduce their value by ~2.6. The real uncertainty would appear to be dominated by systematic uncertainties in porosity corrections and a potential temperature dependence. Given the fact that any porosity correction must reduce the value, a central value of 0.2 is adopted with an uncertainty factor of 2. The high reaction probabilities measured for water ice indicate that this reaction may play a significant role in release of reactive chlorine from the HCl reservoir.

Two studies [Hanson and Ravishankara, [131]; Abbatt and Molina, [5] have measured the reaction probability of HOCl + HCl on NAT surfaces. These data show γ increases as the ambient water pressure increases and then reaches a plateau. At relatively high water pressure, the two studies averaged γo=0.135 ±0.049, with no porosity correction. The reaction probability on water poor NAT-like surfaces falls off dramatically (a factor of 10). A recommendation of 0.1 with and uncertainty factor of 2 is shown in Table A-1. Carslaw and Peter [58] have published a model of this reaction and its dependence on HCl uptake.

41. **HOCl + HCl + H_2SO_4•nH_2O** - This process has been studied in coated flow tubes over ~200-260 K by Zhang et al. [357], Hanson and Ravishankara [134], Donaldson et al. [99], and Hanson and Lovejoy [128]. Hanson and Lovejoy also made measurements in an aerosol flow tube from 251 to 276 K. A model of this and related sulfuric acid aerosol reactions tailored to stratospheric conditions has been published by Hanson et al. [138]. Zhang et al. held the water vapor partial pressure at 3.8 x 10^{-4} torr and showed γ increased by a factor of 50 as the temperature was lowered from 209 to 198 K, showing that the reaction rate is strongly dependent on water activity.

A detailed kinetic uptake model has been developed to fit the experimental data. The formulation for the γ is given as:

$$\frac{1}{\gamma} = \frac{1}{\alpha} + \frac{1}{\Gamma_{HOCl}^{rxn}}$$

where

$$\Gamma_{HOCl}^{rxn} = \frac{4H_{HOCl}RT}{\bar{c}}\left(D_{HOCl}k_{HOCl\_HCl}\right)^{1/2}$$

Over the low temperatures of interest, α for HOCl was assumed to be unity consistent with the value for HCl measured at 240 K and below ([271]). The individual formulations for H_{HOCl}, D_{HOCl} and $k_{HOCl\text{-}HCl}$ are given in the Table A-4 below. Reaction of HOCl with HCl is considered to be acid catalyzed. It is known that the reaction rate for HOCl + HCl in pure water is low [Donaldson et al. [99]]. Experimental data noted above indicated that the reaction rate of HOCl + HCl increases with acidicity of H_2SO_4 solution. The data from the experimental studies noted above were fit to the model without bias. Using the same error analysis discussed in note 17 for N_2O_5, a detailed kinetic model yields a 33.4% error (one sigma fit to the available data set, with σ_m=33.3% and σ_d=3.0%).

In the cold stratosphere where T<190 K, the reaction of $ClONO_2$ + HCl is so fast that HCl is depleted which slows down the reaction of HOCl + HCl. As shown in Table A-4, the effect of HCl depletion on the HOCl reactive uptake coefficient (due to reaction with $ClONO_2$ inside/on the surface of particles) is taken into account via the factor F_{HCl} (also see note 49).

43. **$ClONO_2$ + H_2O(s)** - Measurement of γ = 0.3 (+0.7, -0.1) (Hanson and Ravishankara [130]) significantly exceeds previous measurements of Molina et al. [226], Tolbert et al. [320], Leu [195] and Moore et al. [229] but agrees reasonably well with subsequent measurements by Chu et al. [61] and Zhang et al. [358] when geometrical surface areas are assumed for analysis. Previous measurements were probably complicated by NAT formation on the surface (Hanson and Ravishankara [131]; Chu et al. [61]). Lower levels of $ClONO_2$ (g) used by Hanson and Ravishankara [130] minimized this surface saturation problem. Also, using lower $ClONO_2$ concentrations, Zhang et al. obtained a reaction probability of 0.08 ± 0.02 at 195 K, in fair agreement with the range of 0.03 to 0.13 measured by Chu et al. More recent Knudsen cell measurements at 180 and 200 K by Oppliger et al. [240] showed initial uptake γs in the

0.2 to 0.4 range. Measured reaction products were HNO_3 and HOCl. All of the HNO_3 and much of the HOCl is retained on the surface under polar stratospheric conditions (Hanson and Ravishankara [130,131]). Hanson [124] deposited $ClONO_2$ on $H_2{}^{18}O$ enriched ice and detected $H^{18}OCl$ showing the Cl-ONO2 bond is broken at 191 K.

Data plots confirm a trend showing that at high density of $ClONO_2$, the product HNO_3 covers the ice surface preventing the further reaction of $ClONO_2$ with H_2O molecules on the surface. Therefore, data obtained at high $ClONO_2$ densities (>1014 molecules/cm^3) are excluded from further evaluation. A recent experiment [Berland et al. [30]] using a laser-induced thermal desorption technique yielded a much lower value of $ClONO_2$ reaction probability at 190K (about 3 orders of magnitude lower) after extrapolating the results obtained at temperatures of 140 K and below. We also exclude this point in the averaging of data since the physical characteristics of ice surfaces at these very low temperatures may not be very representative of those found at stratospheric temperatures. Selected data show no temperature dependence between T=180 and 200 K and averaged $\gamma o = 0.28 \pm 0.25$. Again, within the experimental accuracy, the Hanson and Ravishankara [131,132] and Chu et al. [61] data show that uptake measurements are nearly independent of ice substrate thickness. See Henson et al. [141,142] for discussion of a model which accounts for the effect of HNO_3 on the reaction $ClONO_2$ on water and nitric acid ice surfaces.

44. **$ClONO_2 + HNO_3 \bullet nH_2O$** – Hanson and Ravishankara [130] report a value of 0.006 at 201 K for the $ClONO_2$ reaction with the water on NAT ($HNO_3 \bullet nH_2O$). However, these authors present re-analyzed and additional data with $\gamma \approx 0.001$ at 191 K in Hanson and Ravishankara [131,132]. Similar experiments (Moore et al. [229], Leu et al. [199]) report a larger value of 0.02 ± 0.01 which falls very rapidly as slight excesses of H2O above the 3/1 H_2O/HNO_3 ratio for NAT are removed. They measure γ of less than 10-6 for slightly water poor NAT surfaces. The inconsistency between Hanson and Ravishankara and the JPL group (Moore et al. [229]; Leu et al., [199]) has not been resolved. Abbatt and Molina [6] report γ values reaching 0.002 at 202 K and high RH. Hanson and Ravishankara [131] reported that γ for this reaction increases by a factor of 4 as the surface temperature increases from 191 to 211 K. However, Knudsen cell measurements at 185 K by Barone et al. [20] reported $\gamma = 0.004$ at a relative humidity (RH) of 100%, rising to 0.007 near RH = 120%, indicating a possible mild negative temperature dependence when high RH values from this and other studies are compared. Excluding the JPL data, the other data obtained at high RH (~90%) were averaged, assuming no temperature dependence, to yield $\gamma = 0.0043 \pm 0.0021$. The strong dependence on RH and the possible temperature dependence suggest that systematic error probably exceeds the calculated statistical error. Within the experimental accuracy, the data of Hanson and Ravishankara [131,132] show that measured uptake coefficients are independent of ice substrate thickness. Barone et al. report very similar uptake coefficients for nitric acid dihydrate (NAD) as for NAT as a function of RH at 202 K. See Henson et al. [141,142] for discussion of a model which accounts for the effect of HNO_3 on the reaction of $ClONO_2$ on water and nitric acid ice surfaces.

45. **$ClONO_2$ + H_2SO_4•nH_2O(l)** - Results from wetted-wall flow tube [Hanson and Ravishankara [135]] Knudsen cell reactor [Manion et al. [208]] aerosol flow tube [Hanson and Lovejoy [127]], and droplet train uptake [Robinson et al. [272]] experiments supplement older wetted-wall flow tube [Hanson and Ravishankara, [129]] and Knudsen cell measurements [Rossi et al. [273]], [Tolbert et al [319]]. Although earlier Knudsen cell measurements probably suffered from surface saturation, more recent results compare well with those from other techniques. Saturation free results, available over a temperature range of 200-265 K and a H_2SO_4 concentration range of 39 to 75 wt. %, were fit to a phenomenological model developed by Robinson et al. [270]. Measured γ values depend strongly on H_2SO_4 concentration and vary modestly with temperature, with a trend to somewhat higher values for the 210 - 220 temperature range. The temperature-dependent uptake model takes into account the temperature and composition dependence of the effective Henry's Law constant, liquid phase diffusion coefficient, and the liquid phase hydrolysis rate constant. The hydrolysis reaction was treated by modeling two reaction channels, a direct hydrolysis process dominating reaction at low H_2SO_4 concentrations with a reaction rate proportional to water activity and a proton-catalyzed reaction with a rate proportional to H^+ activity, which dominates at higher acid concentrations.

The data fit to the original Robinson et al. model have been supplemented by additional wetted-wall flow tube and aerosol flow tube data from Hanson [125] and aerosol flow tube data from Ball et al. [13]. A revised kinetic model based on Robinson et al. [272] adding these additional data has been developed based on

$$\frac{1}{\gamma} = \frac{1}{\alpha} + \frac{1}{\Gamma_b^{H_2O}}$$

where,

$$\Gamma_b^{H_2O} = \frac{4H_{ClONO_2}RT}{\bar{c}}\left(D_{ClONO_2}k_{hydr}\right)^{1/2}$$

The detailed parameterization for H_{ClONO2}, D_{ClONO2} and k_{hydr} are given in the Appendix. As was the case for N_2O_5 hydrolysis k_{hydr} is seen to have a direct and an acid catalyzed channel. Using the same error analysis approach as in note 17 on N_2O_5 uptake, the error of using the model is about 32.4% (one sigma), with σ_m=32.2% and σ_d=4.0%.

In the calculation of the chlorine activation (Cl_2 production) rate under stratospheric conditions, one needs to take into account the competition between the reactions of $ClONO_2$ + H_2O and $ClONO_2$ + HCl. The presence of HCl will depress the reaction probability of $ClONO_2$ with H_2O (see note 49).

47. **$ClONO_2$ + HCl + H_2O(s)** - Reaction probabilities of 0.27 (+0.73, -0.13) [Leu [195]] and 0.05 to 0.1 [Molina et al. [226]] were reported at 195 and 185 K, respectively. Abbatt and Molina [6] and Hanson and Ravishankara [129] report that a portion of the reaction may be due to HOCl + HCl $\rightarrow$ Cl_2 + H_2O, with HOCl formed from $ClONO_2$ + H_2O(s) $\rightarrow$ HOCl +

HNO_3(s). Hanson and Ravishankara [130] saw no enhancement of the $ClONO_2$ reaction probability when H_2O(s) is doped with HCl. Their preferred value at 192 K is $\gamma = 0.3$, but this is consistent with $\gamma = 1$. Chu et al. [61] also report a value of 0.27 (±0.19) at 188 K, assuming no correction for porosity, but suggest the true value is 0.10 (±0.08). Using a Knudsen cell technique and looking at initial uptake, Oppliger et al. [240] measured $\gamma = 0.7$ at 180 K and 0.2 at 200 K with HCl in excess. Eliminating the Molina et al. points, which were taken at much higher $ClONO_2$ concentrations than the others, data plots of the remaining data show no obvious bias when plotted as a function of reactant concentration or temperature (180-200 K). Their average value $\gamma = 0.26 \pm 0.06$. The Oppliger et al. data were presented for two HCl concentrations, differing by a factor of three. All points from both HCl concentrations were included since all the data were generally consistent with previous measurements, although the higher HCl concentrations did tend to produce modestly higher uptake coefficients. Until a fuller model is available, a single temperature independent value with a moderate uncertainty due to surface porosity seems appropriate.

48. **$ClONO_2$ + HCl + HNO_3•3H_2O** - Measurements by Hanson and Ravishankara [130,131], Leu and co-workers in Moore et al. [229] and Leu et al. [199], and Abbatt and Molina [6] all report high γ values (>0.1) on NAT for temperatures between 192 and 202 K. Hanson and Ravishankara indicate that reaction probabilities on NAD are similar to those on NAT. The most recent NAT studies [Abbatt and Molina [6]] show a strong fall-off with relative humidity from γ >0.2 at 90% RH to 0.002 at 20% RH, indicating the necessity of sufficient water to solvate reactants. Within the limited measurements, data plots show no indication that the reaction probability of $ClONO_2$ + HCl depends on HCl and $ClONO_2$ gas phase concentrations or temperature between 191 and 202 K. Averaged data yield is $\gamma = 0.23$ ±0.10. Carslaw and Peter [58] have published a model of this reaction and its dependence on HCl uptake.

49. **$ClONO_2$ + HCl + H_2SO_4•nH_2O** - Early work by Tolbert et al. [319] and Hanson and Ravishankara [129] indicated that the presence of HCl had little effect on the reaction of $ClONO_2$ with concentrated sulfuric acid (>65 wt.% H_2SO_4). Subsequent realization that HCl would be more soluble, and therefore a more potent reactant, in the colder, more dilute sulfuric acid aerosols characteristic of the polar stratosphere led to additional investigations by Hanson and Ravishankara [135], Zhang et al. [357], Elrod et al. [104] and Hanson [125]. All these measurements show a strong dependence of reactivity on HCl solubility, which in turn depends on water activity. The solubility of HCl in a wide range of sulfuric acid solutions has been experimentally determined by a range of techniques which agree well with current thermodynamic models. See Robinson et al. [271] for a review. Hanson and Lovejoy [127] measured a reacto-diffusive length, ℓ, of only 0.009±0.005 μm for 60 wt.% H_2SO_4 in an aerosol flow reactor. (See Hanson et al. [138] for a definition of ℓ.) This is a factor of four lower than the value for the hydrolysis reaction of $ClONO_2$ showing the significant enhancement of $ClONO_2$ uptake due to HCl.

Since the effect of HCl on the $ClONO_2$ uptake is to increase the $ClONO_2$ pseudo first order reaction rate, the model of $ClONO_2$ uptake (see note 45) should include the pseudo first order reaction rate, k_{HCl}. The formulation of k_{HCl} is found in the Appendix. It is likely that the $ClONO_2$ reaction with HCl, like the $ClONO_2$ hydrolysis reaction, is acid catalyzed

via protonated $HClONO_2^+$, where Cl^+ is activated as in the case of HOCl + HCl. For the $ClONO_2$ + HCl reaction, there is also a surface reaction [Hanson [125]]. Hanson proposed that Γ_s is linearly proportional to water activity; however, the calculated value of γ_o at 250 K and 60 wt% H_2SO_4 using his formulation is 0.02 (here $\gamma_o \sim \Gamma_s$), which is contradictory to his aerosol flow reactor result, which yielded γ_o=0.0079 (here $\gamma_o \sim \Gamma_b$) [Hanson and Lovejoy [127]]. In the model presented in Appendix, it is assumed that that Γ_s is linearly proportional to Henry's law constant of $ClONO_2$, rather than the water activity. The temperature dependence of Γ_s is determined, based on two measured values of Γ_s at 203K [Hanson, [125]] and 250K [Hanson and Lovejoy, [127]]. The proposed model yields a value of $\gamma_o \sim 0.011$ (here $\gamma_o \sim \Gamma_b$), which is close to the measured value. The competition between $ClONO_2$ + HCl and $ClONO_2$ + H_2O is discussed above in note 45. See Table A-3 in the Appendix for the detailed model.

In the stratosphere, when the reaction rate of $ClONO_2$ with HCl exceeds the flux of HCl to the particle surface, HCl is depleted. This, in turn, will depress the rate of both the $ClONO_2$ and HOCl + HCl reactions, and increase the $ClONO_2$ hydrolysis rate. Shi et al. [289] have proposed a model in which this effect is taken into account by including a factor F_{HCl} (see Table A-3). The formulation of F_{HCl} is based on scaling HCl reaction and accommodation fluxes. This flux correction is not exact (i.e. it does rigorously calculate the HCl surface or bulk concentration) but provides a good approximation to expected reduction in HCl + $ClONO_2$/ HOCl reactivity and, just as importantly, the effective increase in $ClONO_2$ + H_2O reactivity when $p_{ClONO2} > p_{HCl}$. This is particularly relevant during cold Cl activation events when HCl can be virtually removed (i.e., see Jaegle et al. [160]).

Using the same error analysis approach as in note 17 on N_2O_5 uptake, the error of using the model in the Appendix is about 40.0% (one sigma), with σ_m=39.8% and σ_d=4.0%.

57. **HOBr + HCl + H_2O(s) and $H_2SO_4 \bullet nH_2O$** - Abbatt [3] measured γ = 0.25 (+0.10/-0.05) for this reaction on ice at 228 K. The BrCl product was observed by mass spectrometry. Since only one value is available, a significantly larger uncertainty than indicated by the stated experimental error is appropriate. No data on NAT surfaces is currently available.

For the sulfuric acid reaction, Abbatt [4] measured γs of ~ 0.1 to 0.2 for [HCl] > 1 x 10^{12} cm^{-3} over 68.8 wt. % H_2SO_4 at 228 K; yielding an estimated $k^{II}_{HCl+HOBr}$ = 1.4 x 10^5 M^{-1} s^{-1} with a factor of 2 uncertainty. Hanson and Ravishankara [136] also measured γ = 0.2 [+0.2, - 0.1] for 60 wt. % H_2SO_4 at 210 K. However, both of these measurements were based on significant underestimation of the solubility of HOBr in the relevant sulfuric acid solutions. More recent measurements by Waschewsky and Abbatt [340] indicate that H for HOBr varies slightly with acidity between 60 to 70 wt.% H_2SO_4 and more strongly with temperature between 208 and 238 K. (For 59.7 wt.% H_2SO_4, H ($M\ atm^{-1}$) = 1.2x10^6 at 208 K and and 2.2x10^5 at 228 K.) The HOBr + HCl second order liquid phase rate constant, $k^{II}_{HCl+HOBr}$, varies between 2x10^5 and 3x10^8 ($M^{-1}s^{-1}$) between 213 and 238 K over the same composition range (60-70 wt.% H_2SO_4). Such a strong dependence on acid composition for the reaction rate of HOBr + HCl and the very small acid composition dependence for HOBr solubility in H_2SO_4 solution might be partially due to the formation of H_2OBr^+ in the acidic solution as discussed in their paper. However, this acid catalyzed reaction, i.e. H_2OBr^+ +

HCl, alone does not completely account for measured reaction rates over the acid composition range studied.

Using the Henry's Law data for HOBr reported by Waschewsky and Abbatt [340], the limiting reagent will vary depending on atmospheric temperature (H_2SO_4 wt.%) and the concentrations of HOBr and HCl. For stratospheric conditions where [HOBr] is 10 pptv and [HCl] 1ppbv, they predict dissolved HOBr will be in excess above 204 K and HCl in excess below 204 K for a H_2O vapor partial pressure of $3x10^{-7}$ atm. From their coated wall flow reactor uptake measurements, Waschewsky and Abbatt [340] derived expressions for $k^{II}_{HCl+HOBr}$ and predicted uptake coefficients. For temperature between 204 and 218 K where HOBr is likely to be in excess, they calculated HCl uptake coefficients, γ_{HCl}, which range between $7x10^{-5}$ and $9x10^{-5}$. For temperatures in the 202-198 K range, where dissolved HCl is likely to be excess, the calculated uptake coefficients for HOBr, γ_{HOBr}, of $\sim 1x10^{-2}$. Clearly, the HOBr + HCl reaction will be difficult to parameterize in a simple manner. Potential inconsistencies in their $k^{II}_{HCl+HOBr}$ values, as discussed by Waschewsky and Abbatt, indicate that further measurements will be required before this reaction can be definitively modeled.

59. **$BrONO_2 + H_2O(s)$** - Hanson and Ravishankara [132] investigated these reactions in an ice-coated flow reactor at 200 (±10) K. The reaction of $BrONO_2$ with $H_2O(s)$ proceeded at a rate indistinguishable from the gas phase diffusion limit, implying that the reaction probability may be as high as one; the product BrNO(g) was observed. Allanic et al [7] used a Knudsen cell reactor to measure $BrONO_2$ uptake between 190-200 K. Values of initial γs in the 0.2-0.3 range were observed. An average $\gamma = 0.26 \pm 0.05$ was obtained from all of the appropriate data from both experiments.

60. **$BrONO_2 + H_2SO_4 \bullet nH_2O$** – Hanson and co-workers used both coated flow tube and aerosol flow tube techniques to show that the reaction of $BrONO_2$ with 45-70 wt. % H_2SO_4 is extremely facile at temperatures from 210 to 298 K. Hanson and Ravishankara [136] measured γs of 0.5 (+ 0.5, - 0.25) (45 wt. % H_2SO_4, 210 K, 0.4 (+0.6, -0.2) (60 wt. %, 210 K) , and 0.3 (+ 0.7, -0.1) (70 wt. %, 220 K) in a coated-wall flow tube experiment. Hanson et al. [137] measured $\gamma \sim 0.8$ (20 to 40% error) for submicron aerosols at temperatures between 249 and 298 K and H_2SO_4 concentrations of 45 to 70 wt. %; they did observe a sharp fall off in γ for H_2SO_4 concentrations between 73 and 83 wt. %. Hanson has analyzed these combined data sets, the data indicated that γ is a function of sulfuric acid concentration, but independent of temperature. He has fit an empirical expression for γ for $BrONO_2 + H_2O$ of: $\gamma = \exp(a+b*wt.)+c$ [Hanson, priv. comm.]. The data have been fitted to the formulation $1/\gamma=1/\alpha+1/\gamma_{rxn}$, yielding $\alpha=0.805$, and $a=29.24$, $b=-0.396$, $c=0.114$. Additional unpublished measurements using both techniques at higher temperatures performed by Hanson [priv. comm.] also fit this functional form. Using the same approach as detailed in note 17 for N_2O_5, the error for $BrONO_2 + H_2O$ is 27.3% (one sigma), with $\sigma_m=26.6\%$ and $\sigma_d=6.3\%$.

APPENDIX

Phenomenological Model of $ClONO_2$ Hydrolysis and the Reaction of $ClONO_2$ and HOCl with HCl in Sulfuric Acid Solutions

In this section, a model is presented which provides a formulation for uptake coefficients for $ClONO_2$ hydrolysis and the reactions of $ClONO_2$ and HOCl with HCl in sulfuric acid solutions. This model is based on the previous work of Robinson et al. [272] and Donaldson et al. [99].

Both $ClONO_2$ and HOCl are protonated ($HClONO_2^+$ and H_2OCl^+) before they react with HCl as was suggested for the reaction of HOCl + HCl by Donaldson et al. [99]. In addition to the normal hydrolysis reaction of $ClONO_2$ with H_2O, there is an acid catalyzed reaction of $ClONO_2$ with H_2O in concentrated H_2SO_4, which involves the intermediate, $HClONO_2^+$. Assuming a steady state for the protonated species, the functional forms for the acid catalyzed reaction rate coefficients of $ClONO_2$ with H_2O, HCl, and HOCl + HCl can be derived. These rate coefficients along with the rate coefficient for $ClONO_2$+ H_2O are obtained via a model fit to experimental data and are listed in the Tables A-3 and A-4. The Henry's Law constant for HOCl in H_2SO_4/H_2O solution is assumed to be dependent on the molarity of H_2SO_4 rather than on the molality of H_2SO_4 as suggested by Huthwelker et al. [158]. The model of Huthwelker et al. underestimated the recently measured values of Donaldson et al. [99]. The new expression for the Henry's law constant for HOCl in Table A-4 was obtained via fitting to previous HOCl solubility data [134] and agrees well with the measurements of Donaldson et al. [99]. A similar expression for $ClONO_2$ solubility is obtained via the model fit to the experimental uptake data. The expressions for HOCl and $ClONO_2$ diffusion coefficients are given by Klassen et al. [181]; however, the viscosity of H_2SO_4/H_2O solution shown in Table A-2 is a new fit.

The following tables present the data needed to calculate the uptake coefficient of $ClONO_2$ + H_2O, HCl, and HOCl + HCl under the stratospheric conditions. Data in Table A-1 were obtained from Tabazadeh et al. [307] and used to calculate the H_2SO_4 weight percentage for a specified temperature, T, and water vapor partial pressure, p_{H2O}. Table A-2 is used to calculate the H_2SO_4 parameters, which are required in the calculation of uptake coefficients. Table A-3 contains the complete uptake model for the reaction of $ClONO_2$ + H_2O and HCl. Table A-4 contains the complete uptake model for the reaction of HOCl + HCl.

Table A-1: Calculations of H_2SO_4 wt.% from T and p_{H2O} (from Tabazadeh et al.[307])

Parameter	Expression			Note
$p^o_{H_2O}$	$\exp\left(18.452406985-\frac{3505.1578807}{T}-\frac{330918.55082}{T^2}+\frac{12725068.262}{T^3}\right)$			saturation water vapor pressure, mbar
aw	$\frac{p_{H_2O}}{p^o_{H_2O}}$			water activity
m	$y_1+\frac{(T-190)(y_2-y_1)}{70}$			H_2SO_4 molality, mol/kg
y_1	$a_1\cdot aw^{b_1}+c_1\cdot aw+d_1$			
y_2	$a_2\cdot aw^{b_2}+c_2\cdot aw+d_2$			
wt.	$\frac{9800\text{m}}{98\text{m}+1000}$			Weight percentage, %
	aw ≤ 0.05 a_1=12.37208932 b_1=-0.16125516114 c_1=-30.490657554 d_1=-2.1133114241 a_2=13.455394705 b_2=-0.1921312255 c_2=-34.285174607 d_2=-1.7620073078	**0.05 < aw < 0.85** a_1=11.820654354 b_1=-0.20786404244 c_1=-4.807306373 d_1=-5.1727540348 a_2=12.891938068 b_2=-0.23233847708 c_2=-6.4261237757 d_2=-4.9005471319	**aw ≥ 0.85** a1=-180.06541028 b1=-0.38601102592 c1=-93.317846778 d1=273.88132245 a2=-176.95814097 b2=-0.36257048154 c2=-90.469744201 d2=267.45509988	

Table A-2: Parameters for H_2SO_4 Solution

Parameter	Value or Expression	References and Note
$M_{H_2SO_4}$	$\frac{\rho \cdot wt}{9.8}$	H_2SO_4 molarity, mol/l
ρ	$1+Z_1 m+Z_2 m^{1.5}+Z_3 m^2$	H_2SO_4 solution density [158], g/cm^3
Z_1	$0.12364-5.6x10^{-7}T^2$	
Z_2	$-0.02954+1.814x10^{-7}T^2$	
Z_3	$2.343x10^{-3}-1.487x10^{-6}T-1.324x10^{-8}T^2$	
X	$\frac{wt}{\left(wt+\frac{(100-wt)98}{18}\right)}$	H_2SO_4 mole fraction
η	$A \cdot T^{-1.43} \exp\left(\frac{448}{(T-T_o)}\right)$	Viscosity of H_2SO_4 solution, cp
A	$169.5+5.18 \cdot wt-0.0825 \cdot wt^2+3.27x10^{-3} wt^3$	
T_o	$144.11+0.166 \cdot wt-0.015 \cdot wt^2+2.18x10^{-4} \cdot wt^3$	
a_H	$\exp[60.51-0.095 \cdot wt+0.0077 \cdot wt^2-1.61x10^{-5} wt^3 -\left(1.76+2.52x10^{-4} \cdot wt^2\right)T^{0.5} +\frac{\left(-805.89+253.05 \cdot wt^{0.076}\right)}{T^{0.5}}]$	Acid activity in molarity

Note: If T and wt. are known, water activity can be calculated from:

$$aw=\exp\left[(-69.775 \cdot X-18253.7 \cdot X^2+31072.2 \cdot X^3-25668.8 \cdot X^4) \cdot \left(\frac{1}{T}-\frac{26.9033}{T^2}\right)\right]$$

Table A-3: Uptake Model Parameters for the $ClONO_2$ + H_2O and $ClONO_2$ + HCl Reactions

Parameter	Value or Expression	References and Notes
$\Gamma_b^{H_2O}$	$\frac{4H_{ClONO_2}RT\left(D_{ClONO_2}k_{hydr}\right)^{0.5}}{C_{ClONO_2}}$	R=0.082 atm $K^{-1}M^{-1}$
C_{ClONO_2}	$1474\cdot T^{0.5}$	$\bar{c}=\left(\frac{8RT}{\pi MW}\right)^{0.5}$, cm s^{-1}
H_{ClONO_2}	$1.6x10^{-6}\cdot\exp\left(\frac{4710}{T}\right)\cdot \exp\left(-S_{ClONO_2}M_{H_2SO_4}\right)$	Shi et al. [289], M atm^{-1}
S_{ClONO_2}	$0.306+\frac{24.0}{T}$	Setchenow coefficient, [289] M^{-1}
D_{ClONO_2}	$\frac{5x10^{-8}T}{\eta}$	Klassen et al.[181], cm^2 s^{-1}
k_{hydr}	$k_{H_2O}a_w+k_Ha_Ha_W$	Shi et al. [289], s^{-1}
k_{H_2O}	$1.95x10^{10}\exp(-2800/T)$	Shi et al. [289], s^{-1}
k_H	$1.22x10^{12}\exp(-6200/T)$	Shi et al. [289], M^{-1} s^{-1}
k_{HCl}	$7.9x10^{11}a_HD_{ClONO_2}M_{HCl}$	[289], s^{-1}
M_{HCl}	$H_{HCl}p_{HCl}$	$p_{HCl}(atm)$, M
H_{HCl}	$\left(0.094-0.61X+1.2X^2\right)\cdot \exp\left(-8.68+\frac{\left(8515-10718\cdot X^{0.7}\right)}{T}\right)$	parameterization of Carslaw et al. [57], M atm^{-1}
ℓ_{ClONO_2}	$\left(\frac{D_{ClONO_2}}{\left(k_{hydr}+k_{HCl}\right)}\right)^{0.5}$	reacto-diffusive length, cm
f_{ClONO_2}	$\frac{1}{\tanh\left(\frac{r}{\ell_{ClONO_2}}\right)}-\frac{\ell_{ClONO_2}}{r}$	r=aerosol radius, cm
$\Gamma_{ClONO_2}^{rxn}$	$f_{ClONO_2}\Gamma_b^{H_2O}\left(1+\frac{k_{HCl}}{k_{hydr}}\right)^{0.5}$	Hanson [125]
Γ_b^{HCl}	$\Gamma_{ClONO_2}^{rxn}\frac{k_{HCl}}{\left(k_{HCl}+k_{hydr}\right)}$	Hanson [125]
Γ_s	$66.12\cdot H_{ClONO_2}M_{HCl}\exp\left(-\frac{1374}{T}\right)$	Shi et al. [289]

Table A-3: Uptake Model Parameters for the $ClONO_2 + H_2O$ and $ClONO_2 + HCl$ Reactions (Cont'd)

F_{HCl}	$\frac{1}{\left(1+\frac{0.612\left(\Gamma_s+\Gamma_b^{HCl}\right)p_{ClONO_2}}{p_{HCl}}\right)}$	$\left(\frac{MW_{HCl}}{MW_{ClONO_2}}\right)^{0.5}=0.612$
Γ_s'	$F_{HCl}\Gamma_s$	
$\Gamma_b^{HCl'}$	$F_{HCl}\Gamma_b^{HCl}$	
Γ_b	$\Gamma_b^{HCl'}+\frac{\Gamma_{ClONO_2}^{rxn}k_{hydr}}{\left(k_{HCl}+k_{hydr}\right)}$	
γ_{ClONO_2}	$\frac{1}{\left(1+\frac{1}{\left(\Gamma_s'+\Gamma_b\right)}\right)}$	
$\gamma_{ClONO_2\_HCl}$	$\gamma_{ClONO_2}\frac{\Gamma_s'+\Gamma_b^{HCl'}}{\Gamma_s'+\Gamma_b}$	Hanson [125]
$\gamma_{ClONO_2\_H_2O}$	$\gamma_{ClONO_2}-\gamma_{ClONO_2\_HCl}$	Hanson [125]

Note: We have assumed that α=1 in Appendix Tables 3 and 4 which is appropriate in the stratosphere. F accounts for depletion of HCl in the particles due to reaction with $ClONO_2$ inside/on the particle surface. The effect of the HOCl + HCl reaction on the HCl concentration has been neglected; however, the depletion of HCl in the particles due to reaction with $ClONO_2$ affects the HOCl + HCl reaction probability which is taken into account through F_{HCl} in Table 4 (see γ_{HOCl}).

Table A-4: Uptake Model Parameters for the HOCl + HCl Reaction

Parameter	Value or Expression	References and Notes
Γ_{HOCl}^{rxn}	$\frac{4H_{HOCl}RT\left(D_{HOCl}k_{HOCl\_HCl}\right)^{0.5}}{C_{HOCl}}$	R=0.082 atm $K^{-1}M^{-1}$
C_{HOCl}	$2009 \cdot T^{0.5}$	$\bar{c}=\left(\frac{8RT}{\pi MW}\right)^{0.5}$, cm s^{-1}
H_{HOCl}	$1.91x10^{-6} \cdot \exp\left(\frac{5862.4}{T}\right) \cdot \exp(-S_{HOCl}M_{H_2SO_4})$	Shi et al. [289]
S_{HOCl}	$0.0776 + \frac{59.18}{T}$	Setchenow coefficient,[289], M^{-1}
D_{HOCl}	$\frac{6.4x10^{-8} \cdot T}{\eta}$	Klassen *et al.*[181], cm^2 s^{-1}
k_{HOCl_HCl}	$1.25x10^{9} a_H D_{HOCl} M_{HCl}$	Shi et al. [289], s^{-1}
ℓ_{HOCl}	$\left(\frac{D_{HOCl}}{k_{HOCl\_HCl}}\right)^{0.5}$	reacto-diffusive length, cm
f_{HOCl}	$\frac{1}{\tanh\left(\frac{r}{\ell_{HOCl}}\right)} - \frac{\ell_{HOCl}}{r}$	r=aerosol radius, cm
γ_{HOCl}	$\frac{1}{\left(1+\frac{1}{\left(f_{HOCl}\Gamma_{HOCl}^{rxn}F_{HOCl}\right)}\right)}$	Shi et al. [289]

Note: The factor F_{HCl} here, as shown in Table A-3, accounts for depletion of HCl in the particles due to reaction with $ClONO_2$ inside/on the particle surface.

REFERENCES

1. Chlorofluoromethanes and the Stratosphere. In *NASA Reference Publication 1010*; Hudson, R. D., Ed.; NASA: Washington, D.C, 1977.
2. The Stratosphere: Present and Future. In *NASA Reference Publication 1049*; Hudson, R. D., Reed, E. I., Eds.; NASA: Washington, D.C, 1979.
3. Abbatt, J. P. D., 1994, Geophys. Res. Lett., **21**, 665-668.
4. Abbatt, J. P. D., 1995, Geophys. Res. Lett., **100**, 14,009-14,017.
5. Abbatt, J. P. D. and M. J. Molina, 1992, Geophys. Res. Lett., **19**, 461-464.
6. Abbatt, J. P. D. and M. J. Molina, 1992, J. Phys. Chem., **96**, 7674-7679.
7. Allanic, A., R. Oppliger and M. Rossi, 1997, J. Geophys. Res., **102**, 23529-23541.
8. Anastasi, C. and I. W. M. Smith, 1976, J. Chem. Soc. Faraday Trans. 2, **72**, 1459-1468.
9. Anderson, J. G., J. J. Margitan and F. Kaufman, 1974, J. Chem. Phys., **60**, 3310.
10. Armerding, W., F. J. Comes and B. Schulke, 1995, J. Phys. Chem., **99**, 3137-3143.
11. Arnold, I., F. J. Comes and G. K. Moortgat, 1977, Chem. Phys., **24**, 211-217.
12. Atkinson, R., D. L. Baulch, R. A. Cox, J. Hampson, R. F., J. A. Kerr, M. J. Rossi and J. Troe, 1997, J. Phys. Chem. Ref. Data, **26**, 1329-1499.
13. Ball, S. M., A. Fried, B. E. Henry and M. Mozurkewich, 1998, Geophys. Res. Lett., **25**, 3339-3342.
14. Ball, S. M. and G. Hancock, 1995, Geophys. Res. Lett., **22**, 1213-1216.
15. Ball, S. M., G. Hancock, S. E. Martin and J. C. Pinot de Moira, 1997, Chem. Phys. Lett., **264**, 531-538.
16. Ball, S. M., G. Hancock, I. J. Murphy and S. P. Rayner, 1993, Geophys. Res. Lett., **20**, 2063-2066.
17. Ball, S. M., G. Hancock, J. C. Pinot de Moira, C. M. Sadowski and F. Winterbottom, 1995, Chem. Phys. Lett., **245**, 1-6.
18. Barnes, R. J., M. Lock, J. Coleman and A. Sinha, 1996, J. Phys. Chem., **100**, 453-457.
19. Barnes, R. J., A. Sinha and H. A. Michelsen, 1998, J. Phys. Chem. A, **102**, 8855-8859.
20. Barone, S. B., M. A. Zondlo and M. A. Tolbert, 1997, J. Phys. Chem. A, **101**, 8643-8652.
21. Basco, N. and S. K. Dogra, 1971, Proc. Roy. Soc. A., **323**, 417-429.
22. Basco, N. and J. E. Hunt, 1979, Int. J. Chem. Kinet., **11**, 649-664.
23. Battin-Leclerc, F., I. K. Kim, R. K. Talukdar, R. W. Portmann, A. R. Ravishankara, R. Steckler and D. Brown, 1999, J. Phys. Chem. A, **103**, 3237-3244.
24. Baulch, D. L., R. A. Cox, P. J. Crutzen, R. F. Hampson, Jr., J. A. Kerr, J. Troe and R. T. Watson, 1982, J. Phys. Chem. Ref. Data, **11**, 327-496.
25. Baulch, D. L., R. A. Cox, R. F. Hampson, Jr., J. A. Kerr, J. Troe and R. T. Watson, 1980, J. Phys. Chem. Ref. Data, **9**, 295-471.
26. Beichert, P., L. Wingen, J. Lee, R. Vogt, M. J. Ezell, M. Ragains, R. Neavyn and B. J. Finlayson-Pitts, 1995, J. Phys. Chem., **99**, 13156-13162.
27. Bemand, P. P., M. A. A. Clyne and R. T. Watson, 1973, J. Chem. Soc. Faraday Trans. 1, **69**, 1356-1374.
28. Bemand, P. P., M. A. A. Clyne and R. T. Watson, 1974, J. Chem. Soc. Faraday Trans. 2, **70**, 564-576.
29. Benter, T., C. Feldmann, U. Kirchner, M. Schmidt, S. Schmidt and R. N. Schindler, 1995, Ber. Bunsenges. Phys. Chem., **99**, 1144-1147.
30. Berland, B. S., M. A. Tolbert and S. M. George, 1997, J. Phys. Chem. A, **101**, 9954-9963.

31. Birk, M., R. R. Friedl, E. A. Cohen, H. M. Pickett and S. P. Sander, 1989, J. Chem. Phys., **91**, 6588-6597.
32. Birks, J. W., B. Shoemaker, T. J. Leck, R. A. Borders and L. J. Hart, 1977, J. Chem. Phys., **66**, 4591-4599.
33. Birks, J. W., B. Shoemaker, T. J. Leck and D. M. Hinton, 1976, J. Chem. Phys., **65**, 5181-5185.
34. Borders, R. A. and J. W. Birks, 1982, J. Phys. Chem., **86**, 3295-3302.
35. Brock, J. C. and R. T. Watson, 1980, Chem. Phys., **46**, 477-484.
36. Brock, J. C. and R. T. Watson, 1980, Chem. Phys. Lett., **71**, 371-375.
37. Brown, S. S., R. K. Talukdar and A. R. Ravishankara, 1999, Chem. Phys. Lett., **299**, 277-284.
38. Brown, S. S., R. K. Talukdar and A. R. Ravishankara, 1999, J. Phys. Chem. A, **103**, 3031-3037.
39. Brune, W. H., J. J. Schwab and J. G. Anderson, 1983, J. Phys. Chem., **87**, 4503-4514.
40. Burkholder, J. B., 1993, J. Geophys. Res., **98**, 2963-2974.
41. Burkholder, J. B., P. D. Hammer and C. J. Howard, 1987, J. Phys. Chem., **91**, 2136-2144.
42. Burkholder, J. B., P. D. Hammer, C. J. Howard and A. Goldman, 1989, J. Geophys. Res., **94**, 2225-2234.
43. Burkholder, J. B., J. J. Orlando and C. J. Howard, 1990, J. Phys. Chem., **94**, 687-695.
44. Burrows, J. P., D. I. Cliff, G. W. Harris, B. A. Thrush and J. P. T. Wilkinson, 1979, Proc. Roy. Soc. (London), **A368**, 463-481.
45. Burrows, J. P., R. A. Cox and R. G. Derwent, 1981, J. Photochem., **16**, 147-168.
46. Burrows, J. P., G. W. Harris and B. A. Thrush, 1977, Nature, **267**, 233-234.
47. Burrows, J. P., G. S. Tyndall and G. K. Moortgat, 1985, Chem. Phys. Lett., **119**, 193-198.
48. Burrows, J. P., G. S. Tyndall and G. K. Moortgat, 1985, J. Phys. Chem., **89**, 4848-4856.
49. Burrows, J. P., T. J. Wallington and R. P. Wayne, 1983, J. Chem. Soc. Faraday Trans. 2, **79**, 111-122.
50. Burrows, J. P., T. J. Wallington and R. P. Wayne, 1984, J. Chem. Soc. Faraday Trans. 2, **80**, 957-971.
51. Butler, P. J. D. and L. F. Phillips, 1983, J. Phys. Chem., **87**, 183-184.
52. Calvert, J. G. and J. N. Pitts. . In *Photochemistry*; John Wiley & Sons, Inc., New York:, 1966; pp 783.
53. Cannon, B. D., J. S. Robertshaw, I. W. M. Smith and M. D. Williams, 1984, Chem. Phys. Lett., **105**, 380-385.
54. Cantrell, C. A., J. A. Davidson, A. H. McDaniel, R. E. Shetter and J. G. Calvert, 1988, J. Chem. Phys., **88**, 4997-5006.
55. Cantrell, C. A., R. E. Shetter and J. G. Calvert, 1994, J. Geophys. Res., **99**, 3739-3743.
56. Cantrell, C. A., R. E. Shetter, J. G. Calvert, G. S. Tyndall and J. J. Orlando, 1993, J. Phys. Chem., **97**, 9141-9148.
57. Carslaw, K. S., S. L. Clegg and P. Brimblecombe, 1995, J. Phys. Chem., **99**, 11,557-11,574.
58. Carslaw, K. S. and T. Peter, 1997, Geophys. Res. Lett., **24**, 1743-1746.
59. Chen, L., H. Rabitz, D. B. Considine, C. H. Jackman and J. A. Shorter, 1997, J. Geophys. Res., **102**, 16,201-16,214.
60. Choo, K. Y. and M. T. Leu, 1985, J. Phys. Chem., **89**, 4832-4837.
61. Chu, L. T., M.-T. Leu and L. F. Keyser, 1993, J. Phys. Chem., **97**, 12798-12804.

62. Clegg, S. L. and P. Brimblecombe, 1986, Atmos. Environ., **20**, 2483.
63. Clough, P. N. and B. A. Thrush, 1967, Trans. Faraday Soc., **63**, 915-925.
64. Clyne, M. A. A. and W. S. Nip, 1976, J. Chem. Soc. Faraday Trans. 1, **72**, 2211-2217.
65. Clyne, M. A. A. and W. S. Nip, 1976, J. Chem. Soc. Faraday Trans. 2, **72**, 838-847.
66. Clyne, M. A. A. and R. F. Walker, 1973, J. Chem. Soc. Faraday Trans. 1, **69**, 1547-1567.
67. Clyne, M. A. A. and R. T. Watson, 1974, J. Chem. Soc. Faraday Trans. 1, **70**, 2250-2259.
68. Clyne, M. A. A. and R. T. Watson, 1977, J. Chem. Soc. Faraday Trans. 1, **73**, 1169-1187.
69. Connell, P. S. and H. S. Johnston, 1979, Geophys. Res. Lett., **6**, 553-556.
70. Cox, R. A., J. P. Burrows and G. B. Coker, 1984, Int. J. Chem. Kinet., **16**, 445-67.
71. Cox, R. A., J. P. Burrows and T. J. Wallington, 1981, Chem. Phys. Lett., **84**, 217-221.
72. Cox, R. A. and R. G. Derwent, 1979, J. Chem. Soc. Far. Trans. 1, **75**, 1635-1647.
73. Cox, R. A. and G. D. Hayman, 1988, Nature, **332**, 796-800.
74. Cox, R. A. and R. Lewis, 1979, J. Chem. Soc. Faraday Trans. 1, **75**, 2649-2661.
75. Croce de Cobos, A. E. and J. Troe, 1984, Int. J. Chem. Kinet., **16**, 1519-1530.
76. Danis, F., F. Caralp, J. Masanet and R. Lesclaux, 1990, Chem. Phys. Lett., **167**, 450.
77. Dasch, W., K.-H. Sternberg and R. N. Schindler, 1981, Ber. Bunsenges. Phys. Chem., **85**, 611-615.
78. Davidson, J. A., C. J. Howard, H. I. Schiff and F. C. Fehsenfeld, 1979, J. Chem. Phys., **70**, 1697-1704.
79. Davis, D. D., J. T. Herron and R. E. Huie, 1973, J. Chem. Phys., **58**, 530-535.
80. DeMore, W. B., 1979, J. Phys. Chem., **83**, 1113-1118.
81. DeMore, W. B. 182nd National Meeting of the American Chemical Society, 1981, New York.
82. DeMore, W. B., 1982, J. Phys. Chem, **86**, 121-126.
83. DeMore, W. B., 1991, J. Geophys. Res., **96**, 4995-5000.
84. DeMore, W. B., D. M. Golden, R. F. Hampson, C. J. Howard, M. J. Kurylo, J. J. Margitan, M. J. Molina, A. R. Ravishankara and R. T. Watson "Chemical Kinetics and Photochemical Data for Use in Stratospheric Modeling, Evaluation Number 7," JPL Publication 85-37, Jet Propulsion Laboratory, California Institute of Technology, Pasadena CA, 1985.
85. DeMore, W. B., D. M. Golden, R. F. Hampson, C. J. Howard, M. J. Kurylo, M. J. Molina, A. R. Ravishankara and S. P. Sander "Chemical Kinetics and Photochemical Data for Use in Stratospheric Modeling, Evaluation Number 8," JPL Publication 87-41, Jet Propulsion Laboratory, California Institute of Technology, Pasadena CA, 1987.
86. DeMore, W. B., D. M. Golden, R. F. Hampson, C. J. Howard, M. J. Kurylo, M. J. Molina, A. R. Ravishankara and S. P. Sander "Chemical Kinetics and Photochemical Data for Use in Stratospheric Modeling, Evaluation Number 9," JPL Publication 90-1, Jet Propulsion Laboratory, California Institute of Technology, Pasadena CA, 1990.
87. DeMore, W. B., D. M. Golden, R. F. Hampson, C. J. Howard, M. J. Kurylo, M. J. Molina, A. R. Ravishankara and S. P. Sander "Chemical Kinetics and Photochemical Data for Use in Stratospheric Modeling, Evaluation Number 10," JPL Publication 92-20, Jet Propulsion Laboratory, California Institute of Technology, Pasadena, CA, 1992.
88. DeMore, W. B., D. M. Golden, R. F. Hampson, C. J. Howard, M. J. Kurylo, M. J. Molina, A. R. Ravishankara and S. P. Sander "Chemical Kinetics and Photochemical Data for Use in Stratospheric Modeling, Evaluation Number 11," JPL Publication 94-26, Jet Propulsion Laboratory, California Institute of Technology, Pasadena, CA, 1994.

89. DeMore, W. B., D. M. Golden, R. F. Hampson, C. J. Howard, M. J. Kurylo, M. J. Molina, A. R. Ravishankara and R. T. Watson "Chemical Kinetics and Photochemical Data for Use in Stratospheric Modeling, Evaluation Number 5," JPL Publication 82-57, Jet Propulsion Laboratory, California Institute of Technology, Pasadena CA, 1982.
90. DeMore, W. B., D. M. Golden, R. F. Hampson, C. J. Howard, M. J. Kurylo, M. J. Molina, A. R. Ravishankara and R. T. Watson "Chemical Kinetics and Photochemical Data for Use in Stratospheric Modeling, Evaluation Number 6," JPL Publication 83-62, Jet Propulsion Laboratory, California Institute of Technology, Pasadena CA, 1983.
91. DeMore, W. B., D. M. Golden, R. F. Hampson, M. J. Kurylo, J. J. Margitan, M. J. Molina, L. J. Stief and R. T. Watson "Chemical Kinetics and Photochemical Data for Use in Stratospheric Modeling, Evaluation Number 4," JPL Publication 81-3, Jet Propulsion Laboratory, California Institute of Technology, Pasadena CA, 1981.
92. DeMore, W. B., S. P. Sander, D. M. Golden, R. F. Hampson, M. J. Kurylo, C. J. Howard, A. R. Ravishankara, C. E. Kolb and M. J. Molina "Chemical Kinetics and Photochemical Data for Use in Stratospheric Modeling, Evaluation Number 12," JPL Publication 97-4, Jet Propulsion Laboratory, California Institute of Technology, Pasadena, CA, 1997.
93. DeMore, W. B., L. J. Stief, F. Kaufman, D. M. Golden, R. F. Hampson, M. J. Kurylo, J. J. Margitan, M. J. Molina and R. T. Watson "Chemical Kinetics and Photochemical Data for Use in Stratospheric Modeling, Evaluation Number 2," JPL Publication 79-27, Jet Propulsion Laboratory, California Institute of Technology, Pasadena, CA, 1979.
94. DeMore, W. B. and E. Tschuikow-Roux, 1990, J. Phys. Chem., **94**, 5856-5860.
95. Deters, B., J. P. Burrows, S. Himmelmann and C. Blindauer, 1996, Ann. Geophysicae, **14**, 468-475.
96. Devolder, P., M. Carlier, J. F. Pauwels and L. R. Sochet, 1984, Chem. Phys. Lett., **111**, 94-99.
97. Dobis, O. and S. W. Benson, 1987, Int. J. Chem. Kinet., **19**, 691-708.
98. Donahue, N. M., M. K. Dubey, R. Mohrschladt, K. Demerjian and J. G. Anderson, 1997, J. Geophys. Res., **102**, 6159-6168.
99. Donaldson, D. J., A. R. Ravishankara and D. R. Hanson, 1997, J. Phys. Chem. A, **101**, 4717-4725.
100. Dransfeld, P. and H. G. Wagner, 1987, Z. Naturforsch., **42a**, 471-476.
101. Dransfield, T. J., K. K. Perkins, N. M. Donahue, J. G. Anderson, M. M. Sprengnether and K. Demerjian, 1999, Geophys. Res. Lett., **26**, 687-690.
102. Dubey, M. K., G. P. Smith, W. S. Hartley, D. E. Kinnison and P. S. Connell, 1997, Geophys. Res. Lett., **24**, 2737-2740.
103. Eberstein, I. J., 1990, Geophys. Res. Lett., **17**, 721-724.
104. Elrod, M. J., R. E. Koch, J. E. Kim and M. S. Molina, 1995, Faraday Discuss, **100**, 269-278.
105. Erler, K., D. Field, R. Zellner and I. W. M. Smith, 1977, Ber. Bunsenges. Phys. Chem., **81**, 22.
106. Fenter, F. F., F. Caloz and M. J. Rossi, 1996, J. Phys. Chem., **100**, 1008-1019.
107. Forster, R., M. Frost, D. Fulle, H. F. Hamann, H. Hippler, Schlepegreli and J. Troe, 1996, J. Chem. Phys., **103**, 2949-2958.
108. Fowles, M., D. N. Mitchell, J. W. L. Morgan and R. P. Wayne, 1982, J. Chem. Soc. Faraday Trans. 2, **78**, 1239-1248.
109. Fox, L. E., D. R. Worsnop, M. S. Zahniser and S. C. Wofsy, 1994, Science, **267**, 351-355.

110. Francisco, J. S., M. R. Hand and I. H. Williams, 1996, J. Phys. Chem., **100**, 9250-9253.
111. Fried, A., B. E. Henry, J. G. Calvert and M. Mozukewich, 1994, J. Geophys. Res., **99**, 3517-3532.
112. Friedl, R. R. and S. P. Sander, 1989, J. Phys. Chem., **93**, 4756-4764.
113. Fulle, D. H., H. F. Hamann, H. Hipler and J. Troe, 1998, J. Chem. Phys., **108**, 5391-5397.
114. Geers-Muller, R. and F. Stuhl, 1987, Chem. Phys. Lett., **135**, 263-268.
115. George, C., J. L. Ponche, P. Mirabel, W. Behnke, V. Sheer and C. Zetzsch, 1994, J. Phys. Chem., **98**, 8780-8784.
116. Gierczak, T., J. B. Burkholder and A. R. Ravishankara, 1999, J. Phys. Chem. A, **103**, 877-883.
117. Glinski, R. J. and J. W. Birks, 1985, J. Phys. Chem., **89**, 3449-3453.
118. Graham, R. A. and H. S. Johnston, 1978, J. Phys. Chem., **82**, 254-268.
119. Greenblatt, G. D. and A. R. Ravishankara, 1990, J. Geophys. Res., **95**, 3539-3547.
120. Hack, W., G. Mex and H. G. Wagner, 1977, Ber. Bunsenges. Phys. Chem., **81**, 677-684.
121. Hack, W., A. W. Preuss, F. Temps and H. G. Wagner, 1979, Ber. Bunsenges. Phys. Chem., **83**, 1275-1279.
122. Handwerk, V. and R. Zellner, 1984, Ber. Bunsenges. Phys. Chem., **88**, 405.
123. Hanning-Lee, M. A., B. B. Brady, L. R. Martin and J. A. Syage, 1996, Geophys. Res. Lett., **23**, 1961-1964.
124. Hanson, D. R., 1995, J. Phys. Chem., **99**, 13,059-13,061.
125. Hanson, D. R., 1998, J. Phys. Chem. A, **102**, 4794-4807.
126. Hanson, D. R. and E. R. Lovejoy, 1994, Geophys. Res. Lett., **21**, 2401-2404.
127. Hanson, D. R. and E. R. Lovejoy, 1995, Science, **267**, 1326-1329.
128. Hanson, D. R. and E. R. Lovejoy, 1996, J. Phys. Chem., **100**, 6397-6405.
129. Hanson, D. R. and A. R. Ravishankara, 1991, J. Geophys. Res., **96**, 17307-17314.
130. Hanson, D. R. and A. R. Ravishankara, 1991, J. Geophys. Res., **96**, 5081-5090.
131. Hanson, D. R. and A. R. Ravishankara, 1992, J. Phys. Chem., **96**, 2682-2691.
132. Hanson, D. R. and A. R. Ravishankara, 1993, J. Phys. Chem., **97**, 2802-2803.
133. Hanson, D. R. and A. R. Ravishankara, 1993, J. Geophys. Res., **98**, 22931-22936.
134. Hanson, D. R. and A. R. Ravishankara, 1993, J. Phys. Chem., **97**, 12309-12319.
135. Hanson, D. R. and A. R. Ravishankara, 1994, J. Phys. Chem., **98**, 5728-5735.
136. Hanson, D. R. and A. R. Ravishankara, 1995, Geophys. Res. Lett., **22**, 385-388.
137. Hanson, D. R., A. R. Ravishankara and E. R. Lovejoy, 1996, J. Geophys. Res., **101**, 9063-9069.
138. Hanson, D. R., A. R. Ravishankara and S. Solomon, 1994, J. Geophys. Res., **99**, 3615-3629.
139. Hayman, G. D., J. M. Davies and R. A. Cox, 1986, Geophys. Res. Lett., **13**, 1347-1350.
140. Heneghan, S. P., P. A. Knoot and S. W. Benson, 1981, Int. J. Chem. Kinet., **13**, 677-691.
141. Henson, B. F., K. R. Wilson and J. M. Robinson, 1996, Geophys. Res. Lett., **23**, 1021-1024.
142. Henson, B. F., K. R. Wilson and J. M. Robinson, 1999, submitted to J. Phys. Chem. A, .
143. Hills, A. J., R. J. Cicerone, J. G. Calvert and J. W. Birks, 1988, J. Phys. Chem., **92**, 1853-1858.
144. Hills, A. J. and C. J. Howard, 1984, J. Chem. Phys., **81**, 4458-4465.
145. Hippler, H., M. Siefke, H. Stark and J. Troe, 1999, Phys. Chem. Chem. Phys., **1**, 57-61.
146. Hippler, H. and J. Troe, 1992, Chem. Phys. Lett., **192**, 333-337.

147. Hjorth, J., J. Nothholt and G. Restelli, 1992, Int. J. Chem. Kinet., **24**, 51-65.
148. Hochanadel, C. J., T. J. Sworski and P. J. Ogren, 1980, J. Phys. Chem., **84**, 3274-3277.
149. Hofmann, D. J. and S. J. Oltmans, 1992, Geophys. Res. Lett., **22**, 2211-2214.
150. Horowitz, A., J. N. Crowley and G. K. Moortgat, 1994, J. Phys. Chem., **98**, 11924-11930.
151. Howard, C. J. and K. M. Evenson, 1974, J. Chem. Phys., **61**, 1943.
152. Hu, J. H. and J. P. D. Abbatt, 1997, J. Phys. Chem. A, **101**, 871-878.
153. Hu, J. H., Q. Shi, P. Davidovits, D. R. Worsnop, M. S. Zahniser and C. E. Kolb, 1995, J. Phys. Chem., **99**, 8768-8776.
154. Huder, K. J. and W. B. DeMore, 1995, J. Phys. Chem., **99**, 3905-3908.
155. Hudson, R. D., 1971, Reviews of Geophysics and Space Physics, **9**, 305-399.
156. Husain, D., J. M. C. Plane and N. K. H. Slater, 1981, J. Chem. Soc. Faraday Trans. 2, **77**, 1949-1962.
157. Husain, D., J. M. C. Plane and C. C. Xiang, 1984, J. Chem. Soc. Faraday Trans. 2, **80**, 713-728.
158. Huthwelker, T., T. Peter, B. P. Juo, S. L. Clegg, K. S. Carshlaw and P. Brimblecombe, 1995, J. Atmos. Chem., **21**, 81-95.
159. Ingham, T., D. Bauer, J. Landgraf and J. N. Crowley, 1998, J. Phys. Chem. A, **102**, 3293-3298.
160. Jaegle, L., C. R. Webster, R. D. May, D. C. Scott, R. M. Stimpfle, D. W. Kohn, P. O. Wennberg, T. F. Hansico, R. C. Cohen, M. H. Proffitt, K. K. Kelly, J. Elkins, D. Baumgardner, J. E. Dye, J. C. Wilson, R. F. Pueschel, K. R. Chan, R. J. Salawitch, A. F. Tuck, S. J. Hovde and Y. L. Yung, 1997, J. Geophys. Res., **102**, 13,235-13,253.
161. Jayne, J. T., D. R. Worsnop, C. E. Kolb, E. Swartz and P. Davidovits, 1996, J. Phys. Chem., **100**, 8015-8022.
162. Jensen, F. and J. Oddershede, 1990, J. Phys. Chem., **94**, 2235.
163. Johnston, H. S., C. A. Cantrell and J. G. Calvert, 1986, J. Geophys. Res., **91**, 5159-5172.
164. Johnston, H. S., E. D. Morris, Jr. and J. Van den Bogaerde, 1969, J. Am. Chem. Soc., **91**, 7712-7727.
165. Jungkamp, T. P. W., U. Kirchner, M. Schmidt and R. N. Schindler, 1995, J. Photochem. Photobiol. A: Chemistry, **99**, 1-6.
166. Kaye, J. A., 1986, J. Geophys. Res., **91**, 7865-7874.
167. Kegley-Owen, C. S., M. K. Gilles, J. B. Burkholder and A. R. Ravishankara, 1999, J. Phys. Chem. A, **103**, 5040-5048.
168. Keyser, L. F., 1978, J. Chem. Phys., **69**, 214-218.
169. Keyser, L. F., 1981, J. Phys. Chem., **85**, 3667-3673.
170. Keyser, L. F., 1982, J. Phys. Chem., **86**, 3439-3446.
171. Keyser, L. F., 1983, J. Phys. Chem., **87**, 837-841.
172. Keyser, L. F., 1984, J. Phys. Chem., **88**, 4750-4758.
173. Keyser, L. F., 1988, J. Phys. Chem., **92**, 1193-1200.
174. Keyser, L. F., K. Y. Choo and M. T. Leu, 1985, Int. J. Chem. Kinet., **17**, 1169-1185.
175. Keyser, L. F. and M.-T. Leu, 1993, J. Colloid Interface Sci., **155**, 137-145.
176. Keyser, L. F. and M.-T. Leu, 1993, Micros. Res. Technol., **25**, 434-438.
177. Keyser, L. F., M.-T. Leu and S. B. Moore, 1993, J. Phys. Chem., **97**, 2800-2801.
178. Keyser, L. F., S. B. Moore and M. T. Leu, 1991, J. Phys. Chem., **95**, 5496-5502.
179. Kircher, C. C., J. J. Margitan and S. P. Sander, 1984, J. Phys. Chem., **88**, 4370-4375.
180. Klais, O., P. C. Anderson and M. J. Kurylo, 1980, Int. J. Chem. Kinet., **12**, 469-490.

181. Klassen, J. K., Z. Hu and L. R. Williams, 1998, J. Geophys. Res., **103**, 16,197-16,202.
182. Knauth, H. D., H. Alberti and H. Clausen, 1979, J. Phys. Chem., **83**, 1604-1612.
183. Knox, J. H., 1955, Chemistry and Industry, 1631-1632.
184. Knox, J. H. and R. L. Nelson, 1959, Trans. Far. Soc., **55**, 937-946.
185. Kolb, C. E., D. R. Worsnop, M. S. Zahniser, P. Davidovits, L. F. Keyser, M.-T. Leu, M. J. Molina, D. R. Hanson, A. R. Ravishankara, L. R. Williams and M. A. Tolbert. Progress and Problems in Atmospheric Chemistry. In *Adv. Phys. Chem. Series, 3*; Barker, J. R., Ed., 1994; pp 771-875.
186. Kulcke, A., B. Blackman, W. B. Chapman, I. K. Kim and D. J. Nesbitt, 1998, J. Phys. Chem. A, **102**, 1965-1972.
187. Kurylo, M. J., 1973, Chem. Phys. Lett., **23**, 467-471.
188. Kurylo, M. J. and W. Braun, 1976, Chem. Phys. Lett., **37**, 232-235.
189. Kurylo, M. J., O. Klais and A. H. Laufer, 1981, J. Phys. Chem., **85**, 3674-3678.
190. Lam, L., D. R. Hastie, B. A. Ridley and H. I. Schiff, 1981, J. Photochem., **15**, 119-130.
191. Lee, F. S. C. and F. S. Rowland, 1977, J. Phys. Chem., **81**, 86-87.
192. Lee, T. J., C. M. Rohlfing and J. E. Rice, 1992, J. Chem. Phys., **97**, 6593-6605.
193. Lee, Y.-P., R. M. Stimpfle, R. A. Perry, J. A. Mucha, K. M. Evenson, D. A. Jennings and C. J. Howard, 1982, Int. J. Chem. Kinet., **14**, 711-732.
194. Leu, M. T., 1984, J. Phys. Chem., **88**, 1394-1398.
195. Leu, M. T., 1988, Geophys. Res. Lett., **15**, 17-20.
196. Leu, M. T. and W. B. DeMore, 1976, Chem. Phys. Lett. , **41**, 121-124.
197. Leu, M. T. and C. L. Lin, 1979, Geophys. Res. Lett., **6**, 425-428.
198. Leu, M. T., C. L. Lin and W. B. DeMore, 1977, J. Phys. Chem., **81**, 190-195.
199. Leu, M. T., S. B. Moore and L. F. Keyser, 1991, J. Phys. Chem., **95**, 7763-7771.
200. Leu, M. T. and Y. L. Yung, 1987, Geophys. Res. Lett., **14**, 949-952.
201. Lii, R.-R., R. A. Gorse, Jr., M. C. Sauer, Jr. and S. Gordon, 1980, J. Phys. Chem., **84**, 819-821.
202. Lin, C. L. and M. T. Leu, 1982, Int. J. Chem. Kinet., **14**, 417.
203. Lin, C. L., M. T. Leu and W. B. DeMore, 1978, J. Phys. Chem., **82**, 1772-1777.
204. Lippmann, H. H., B. Jesser and U. Schurath, 1980, Int. J. Chem. Kinet., **12**, 547-554.
205. Lipson, J. B., T. W. Beiderhase, L. T. Molina, M. J. Molina and M. Olzmann, 1999, J. Phys. Chem. A, **103**, 6540-6551.
206. Lipson, J. B., M. J. Elrod, T. W. Beiderhase, L. T. Molina and M. J. Molina, 1997, J. Chem. Soc. Faraday Trans., **93**, 2665-2673.
207. Lock, M., R. J. Barmes and A. Sinha, 1996, J. Phys. Chem., **100**, 7972-7980.
208. Manion, J. A., C. M. Fittschen, D. M. Golden, L. R. Williams and M. A. Tolbert, 1994, Israel J. Chem., **34**, 355-363.
209. Manning, R. and M. J. Kurylo, 1977, J. Phys. Chem., **81**, 291-296.
210. Manzanares, E. R., M. Suto, L. C. Lee and D. Coffey, 1986, J. Chem. Phys., **85**, 5027-5034.
211. Margitan, J. J., 1984, J. Phys. Chem., **88**, 3638-3643.
212. Margitan, J. J. and R. T. Watson, 1982, J. Phys. Chem., **86**, 3819-3824.
213. Marx, W., F. Bahe and U. Schurath, 1979, Ber. Bunsenges. Phys. Chem., **83**, 225-230.
214. McGrath, M. P., K. C. Clemitshaw, F. S. Rowland and W. J. Hehre, 1988, Geophys. Res. Lett., **15**, 883-886.

215. McGrath, M. P., K. C. Clemitshaw, F. S. Rowland and W. J. Hehre, 1990, J. Phys. Chem., **94**, 6126-6132.
216. Michael, J. V., J. E. Allen, Jr. and W. D. Brobst, 1981, J. Phys. Chem., **85**, 4109-4117.
217. Michael, J. V. and J. H. Lee, 1977, Chem. Phys. Lett., **51**, 303-306.
218. Michelangeli, D. V., M. Allen and Y. L. Yung, 1991, Geophys. Res. Lett., **18**, 673-676.
219. Middlebrook, A. M., L. T. Iraci, L. S. McNeil, B. G. Koehler, M. A. Wilson, O. W. Saastad and M. A. Tolbert, 1993, J. Geophys. Res., **98**, 20473-20481.
220. Mishalanie, E. A., J. C. Rutkowski, R. S. Hutte and J. W. Birks, 1986, J. Phys. Chem., **90**, 5578-5584.
221. Molina, L. T. and M. J. Molina, 1978, J. Phys. Chem., **82**, 2410-2414.
222. Molina, M. J., A. J. Colussi, L. T. Molina, R. N. Schindler and T. L. Tso, 1990, Chem. Phys. Lett., **173**, 310-315.
223. Molina, M. J., T. Ishiwata and L. T. Molina, 1980, J. Phys. Chem., **84**, 821-826.
224. Molina, M. J., L. T. Molina and T. Ishiwata, 1980, J. Phys. Chem., **84**, 3100-3104.
225. Molina, M. J., L. T. Molina and C. A. Smith, 1984, Int. J. Chem. Kinet., **16**, 1151-1160.
226. Molina, M. J., T. L. Tso, L. T. Molina and F. C. Wang, 1987, Science, **238**, 1253-1259.
227. Molina, M. J., R. Zhang, P. J. Woolridge, J. R. McMahon, J. E. Kim, H. Y. Chang and K. D. Beyer, 1993, Science, **261**, 1418-1423.
228. Moonen, P. C., J. N. Cape, R. L. Storeton-West and R. McColm, 1998, J. Atmos. Chem., **29**, 299-314.
229. Moore, S. B., L. F. Keyser, M. T. Leu, R. P. Turco and R. H. Smith, 1990, Nature, **345**, 333-335.
230. Moore, T. A., M. Okumura, J. W. Seale and T. K. Minton, 1999, J. Phys. Chem. A, **103**, 1692-1695.
231. Mozurkewich, M. and J. Calvert, 1988, J. Geophys. Res., **93**, 889-896.
232. Msibi, I. M., Y. Li, J. P. Shi and R. M. Harrison, 1994, J. Phys. Chem., **18**, 291-300.
233. Nelson, D. D., Jr. and M. S. Zahniser, 1994, J. Phys. Chem., **98**, 2101-2104.
234. Nickolaisen, S. L., R. R. Friedl and S. P. Sander, 1994, J. Phys. Chem., **98**, 155-169.
235. Nicovich, J. M., K. D. Kreutter and P. H. Wine, 1990, Int. J Chem. Kinet., **22**, 399-414.
236. Nicovich, J. M. and P. H. Wine, 1987, J. Phys. Chem., **91**, 5118-5123.
237. Nicovich, J. M., P. H. Wine and A. R. Ravishankara, 1988, J. Chem. Phys., **89**, 5670-5679.
238. Ongstad, A. P. and J. W. Birks, 1984, J. Chem. Phys., **81**, 3922-3930.
239. Ongstad, A. P. and J. W. Birks, 1986, J. Chem. Phys., **85**, 3359-3368.
240. Oppliger, R., A. Allanic and M. J. Rossi, 1997, J. Phys. Chem. A, **101**, 1903-1911.
241. Orlando, J. J. and J. B. Burkholder, 1995, J. Phys. Chem., **99**, 1143-1150.
242. Orlando, J. J. and G. S. Tyndall, 1996, J. Phys. Chem., **100**, 19398-19405.
243. Orlando, J. J., G. S. Tyndall, C. A. Cantrell and J. G. Calvert, 1991, J. Chem. Soc. Far. Trans., **87**, 2345-2349.
244. Parthiban, P. and T. Lee, 1998, J. Chem. Phys., **109**, 525-530.
245. Patrick, R. and D. M. Golden, 1983, Int. J. Chem. Kinet., **15**, 1189-1227.
246. Paulson, S. E., J. J. Orlando, G. S. Tyndall and J. G. Calvert, 1995, Int. J. Chem. Kinet., **27**, 997-1008.
247. Percival, C. J., G. D. Smith, L. T. Molina and M. J. Molina, 1997, J. Phys. Chem. A, **101**, 8830-8833.

248. Permien, T., R. Vogt and R. N. Schindler. Mechanisms of Gas Phase-Liquid Phase Chemical Transformations. In *Air Pollution Report #17*; Cox, R. A., Ed.; Environmental Research Program of the CEC.: Brussels, 1988.
249. Perner, D., A. Schmeltekopf, R. H. Winkler, H. S. Johnston, J. G. Calvert, C. A. Cantrell and W. R. Stockwell, 1985, J. Geophys. Res., **90**, 3807-3812.
250. Pilgrim, J. S., A. McIlroy and C. A. Taatjes, 1997, J. Phys. Chem. A, **101**, 1873-1880.
251. Poulet, G., I. T. Lancar, G. Laverdet and G. Le Bras, 1990, J. Phys. Chem., **94**, 278-284.
252. Poulet, G., G. Laverdet and G. Le Bras, 1986, J. Phys. Chem., **90**, 159-165.
253. Poulet, G., G. Le Bras and J. Combourieu, 1974, J. Chim. Physique, **71**, 101-106.
254. Pritchard, H. O., 1994, Int. J. Chem. Kinet., **26**, 61-72.
255. Pritchard, H. O., J. B. Pyke and A. F. Trotman-Dickenson, 1954, J. Amer. Chem. Soc., **76**, 1201-1202.
256. Pritchard, H. O., J. B. Pyke and A. F. Trotman-Dickenson, 1955, J. Amer. Chem. Soc., **77**, 2629-2633.
257. Pueschel, R. F., D. F. Blake, A. G. Suetsinger, A. D. A. Hansen, S. Verma and K. Kato, 1992, Geophys. Res. Lett., **19**, 1659-1662.
258. Quinlan, M. A., C. M. Reihs, D. M. Golden and M. A. Tolbert, 1990, J. Phys. Chem., **94**, 3255-3260.
259. Rattigan, O. V., D. J. Lary, R. L. Jones and R. A. Cox, 1996, J. Geophys. Res., **101**, 23021-23033.
260. Ravishankara, A. R., F. L. Eisele and P. H. Wine, 1983, J. Chem. Phys., **78**, 1140-1144.
261. Ravishankara, A. R., G. Smith, R. T. Watson and D. D. Davis, 1977, J. Phys. Chem., **81**, 2220-2225.
262. Ravishankara, A. R. and P. H. Wine, 1980, J. Chem. Phys., **72**, 25-30.
263. Ravishankara, A. R., P. H. Wine and A. O. Langford, 1979, J. Chem. Phys., **70**, 984-989.
264. Ravishankara, A. R., P. H. Wine and J. M. Nicovich, 1983, J. Chem. Phys., **78**, 6629-6639.
265. Ravishankara, A. R., P. H. Wine, J. R. Wells and R. L. Thompson, 1985, Int. J. Chem. Kinet., **17**, 1281-1297.
266. Rawlins, W. T., G. E. Caledonia and R. A. Armstrong, 1987, J. Chem. Phys ., **87**, 5209-5213 .
267. Ray, G. W. and R. T. Watson, 1981, J. Phys. Chem., **85** , 1673-1676.
268. Rayez, M. T. and M. Destriau, 1993, Chem. Phys. Lett., **206**, 278-284.
269. Robertshaw, J. S. and I. W. M. Smith, 1982, J. Phys. Chem., **86**, 785.
270. Robinson, G. N., D. R. Worsnop, J. T. Jayne, C. E. Kolb and P. Davidovits, 1996, J. Geophys. Res., **102**, 3583-3601.
271. Robinson, G. N., D. R. Worsnop, J. T. Jayne, C. E. Kolb, E. Swartz and P. Davidovits, 1998, J. Geophys. Res., **103**, 25,371-25,381.
272. Robinson, G. N., D. R. Worsonop, J. T. Jayne, C. E. Kolb and P. Davidovits, 1997, J. Geophys. Res., **102**, 3583-3601.
273. Rossi, M. J., R. Malhotra and D. M. Golden, 1987, Geophys. Res. Lett., **14**, 127-130.
274. Rozenshtein, V. B., Y. M. Gershenzon, S. O. Il'in and O. P. Kishkovitch, 1984, Chem. Phys. Lett., **112**, 473-478.
275. Sander, S. P., R. P. Friedl and Y. L. Yung, 1989, Science, **245**, 1095-1098.
276. Sander, S. P. and R. R. Friedl, 1989, J. Phys. Chem., **93**, 4764-4771.

277. Sander, S. P., R. R. Friedl, W. B. DeMore, D. M. Golden, M. J. Kurylo, R. F. Hampson, R. E. Huie, G. K. Moortgat, A. R. Ravishankara, C. E. Kolb and M. J. Molina "Chemical Kinetics and Photochemical Data for Use in Stratospheric Modeling, Evaluation Number 13," JPL Publication 00-3, Jet Propulsion Laboratory, California Institute of Technology, Pasadena, CA, 2000.
278. Sander, S. P., G. W. Ray and R. T. Watson, 1981, J. Phys. Chem., **85**, 199.
279. Sawerysyn, J.-P., C. Lafage, B. Meriaux and A. Tighezza, 1987, J. Chim. Phys., **84**, 1187-1193.
280. Schieferstein, M., K. Kohse-Höinghaus and F. Stuhl, 1983, Ber. Bunsenges. Phys. Chem., **87**, 361-366.
281. Schott, G. and N. Davidson, 1958, J. Amer. Chem. Soc., **80**, 1841-1853.
282. Schurath, U., H. H. Lippmann and B. Jesser, 1981, Ber. Bunsenges. Phys. Chem., **85**, 807-813.
283. Schwab, J. J., W. H. Brune and J. G. Anderson, 1989, J. Phys. Chem., **93**, 1030-1035.
284. Schwab, J. J., D. W. Toohey, W. H. Brune and J. G. Anderson, 1984, J. Geophys. Res., **89**, 9581-9587.
285. Schwartz, S. E., 1988, Atmos. Environ., **22**, 2331.
286. Schweitzer, F., P. Mirabel and C. George, 1998, J. Phys. Chem. A, **102**, 3942-3952.
287. Seeley, J. V., J. T. Jayne and M. J. Molina, 1996, J. Phys. Chem., **100**, 4019-4025.
288. Sharkey, P. and I. W. M. Smith, 1993, J. Chem. Soc. Faraday Trans., **89**, 631-638.
289. Shi, Q., P. Davidovits, J. T. Jayne, C. E. Kolb and D. R. Worsnop, 2000, submitted to J. Geophys. Res., .
290. Silvente, E., R. C. Richter, M. Zheng, E. S. Saltzman and A. J. Hynes, 1997, Chem. Phys. Lett., **264**, 309-315.
291. Sinha, A., E. R. Lovejoy and C. J. Howard, 1987, J. Chem. Phys., **87**, 2122-2128.
292. Slanger, T. G., B. J. Wood and G. Black, 1973, Int. J. Chem. Kinet., **5**, 615-620.
293. Slanina, Z. and F. Uhlik, 1991, Chem. Phys. Lett., **182**, 51-56.
294. Smith, C. A., L. T. Molina, J. J. Lamb and M. J. Molina, 1984, Int. J. Chem. Kinet., **16**, 41-55.
295. Smith, C. A., A. R. Ravishankara and P. H. Wine, 1985, J. Phys. Chem., **89**, 1423-1427.
296. Smith, G. P. and D. M. Golden, 1978, Int. J. Chem. Kinet., **10**, 489-501.
297. Smith, I. W. M. and M. D. Williams, 1986, J. Chem. Soc. Faraday Trans. 2, **82**, 1043-1055.
298. Smith, I. W. M. and R. Zellner, 1974, J. Chem. Soc.. Faraday Trans. 2, **70**, 1045-1056.
299. Sridharan, U. C., F. S. Klein and F. Kaufman, 1985, J. Chem. Phys., **82**, 592-593.
300. Sridharan, U. C., L. X. Qiu and F. Kaufman, 1981, J. Phys. Chem., **85**, 3361-3363.
301. Sridharan, U. C., L. X. Qiu and F. Kaufman, 1982, J. Phys. Chem., **86**, 4569-4574.
302. Sridharan, U. C., L. X. Qiu and F. Kaufman, 1984, J. Phys. Chem., **88**, 1281-1282.
303. Stachnik, R. A., M. J. Molina and L. T. Molina, 1986, J. Phys. Chem., **90**, 2777-2780.
304. Stanton, J. F. and R. J. Bartlett, 1993, J. Chem. Phys., **98**, 9335-9339.
305. Stanton, J. F., C. M. L. Rittby, R. J. Bartlett and D. W. Toohey, 1991, J. Phys. Chem., **95**, 2107-2110.
306. Stedman, D. H. and H. Niki, 1973, J. Phys. Chem., **77**, 2604-2609.
307. Tabazadeh, A., O. B. Toon, S. L. Clegg and P. Hammill, 1997, Geophys. Res. Lett., **24**, 1931-1934.
308. Takacs, G. A. and G. P. Glass, 1973, J. Phys. Chem., **77**, 1948-1951.

309. Takahashi, K., M. Kishigami, Y. Matsumi, M. Kawasaki and A. J. Orr-Ewing, 1996, J. Chem. Phys., **105**, 5290-5293.
310. Takahashi, K., M. Kishigami, N. Taniguchi, Y. Matsumi and M. Kawasaki, 1997, J. Chem. Phys., **106**, 6390-6397.
311. Takahashi, K., Y. Matsumi and M. Kawasaki, 1996, J. Phys. Chem., **100**, 4084-4089.
312. Takahashi, K., R. Wada, Y. Matsumi and M. Kawasaki, 1996, J. Phys. Chem., **100**, 10145-10149.
313. Talukdar, R. K., M. K. Gilles, F. Battin-Leclerc, A. R. Ravishankara, J.-M. Fracheboud, J. J. Orlando and G. S. Tyndall, 1997, Geophys. Res. Lett., **24**, 1091-1094.
314. Talukdar, R. K., C. A. Longfellow, M. K. Gilles and A. R. Ravishankara, 1998, Geophys. Res. lett., **25**, 143-146.
315. Temps, F. and H. G. Wagner, 1982, Ber. Bunsenges. Phys. Chem., **86**, 119-125.
316. Thompson, A. M. and R. W. Stewart, 1991, J. Geophys. Res., **96**, 13,089-13,108.
317. Thorn, R. P., E. P. Daykin and P. H. Wine, 1993, Int J. Chem. Kinet., **25**, 521-537.
318. Thrush, B. A. and J. P. T. Wilkinson, 1981, Chem. Phys. Lett., **81**, 1-3.
319. Tolbert, M. A., M. J. Rossi and D. M. Golden, 1988, Geophys. Res. Lett., **15**, 847-850.
320. Tolbert, M. A., M. J. Rossi, R. Malhotra and D. M. Golden, 1987, Science, **238**, 1258-1260.
321. Toohey, D. W. and J. G. Anderson, 1988, J. Phys. Chem., **92**, 1705-1708.
322. Toon, O., E. Browell, B. Gray, L. Lait, J. Livingston, P. Newman, R. P. P. Russell, M. Schoeberl, G. Toon, W. Traub, F. P. J. Valero, H. Selkirk and J. Jordan, 1993, Science, **261**, 1136-1140.
323. Troe, J., 1977, J. Chem. Phys., **66**, 4745 .
324. Trolier, M., R. L. Mauldin, III and A. R. Ravishankara, 1990, J. Phys. Chem., **94**, 4896-4907.
325. Trolier, M. and J. R. Wiesenfeld, 1988, J. Geophys. Res., **93**, 7119-7124.
326. Tuazon, E. C., E. Sanhueza, R. Atkinson, W. P. L. Carter, A. M. Winer and J. N. Pitts, Jr., 1984, J. Phys. Chem., **88**, 3095-3098.
327. Turnipseed, A. A., J. W. Birks and J. G. Calvert, 1991, J. Phys. Chem., **95**, 4356-4364.
328. Van Doren, J. M., L. R. Watson, P. Davidovits, D. R. Worsnop, M. S. Zahniser and C. E. Kolb, 1990, J. Phys. Chem., **94**, 3265-3269.
329. Van Doren, J. M., L. R. Watson, P. Davidovits, D. R. Worsnop, M. S. Zahniser and C. E. Kolb, 1991, J. Phys. Chem., **95**, 1684-1689.
330. Vanderzanden, J. W. and J. W. Birks, 1982, Chem. Phys. Lett., **88**, 109-114.
331. Viggiano, A. A., J. A. Davidson, F. C. Fehsenfeld and E. E. Ferguson, 1981, J. Chem. Phys., **74**, 6113-6125.
332. Vogt, R. and R. N. Schindler, 1992, J. Photochem. Photobiol. A: Chem., **66**, 133-140.
333. Volltrauer, H. N., W. Felder, R. J. Pirkle and A. Fontijn, 1979, J. Photochem., **11**, 173-181.
334. Walker, R. W. . In *Ph.D. Thesis*; Queen Mary College University of London:, 1972.
335. Wallington, T. J., R. Atkinson, A. M. Winer and J. N. Pitts, Jr., 1987, Int. J. Chem. Kinet., **19**, 243-249.
336. Wallington, T. J. and R. A. Cox, 1986, J. Chem. Soc. Faraday Trans. 2, **82**, 275-289.
337. Wang, X., M. Suto and L. C. Lee, 1988, J. Chem. Phys., **88** , 896-899.
338. Wangberg, I., T. Etzkorn, I. Barnes, U. Platt and K. H. Becker, 1997, J. Phys. Chem. A, **101**, 9694-9698.

339. Wangberg, I., E. Ljungstrom, B. E. R. Olsson and J. Davidsson, 1992, J. Phys. Chem., **96**, 7640-7645.
340. Waschewsky, G. C. G. and J. P. D. Abbatt, 1999, J. Phys. Chem. A, **103**, 5312-5320.
341. Watson, L. R., J. M. V. Doren, P. Davidovits, D. R. Worsnop, M. S. Zahniser and C. E. Kolb, 1990, J. Geophys. Res., **95**, 5631-5638.
342. Watson, R. T., G. Machado, S. Fischer and D. D. Davis, 1976, J. Chem. Phys., **65**, 2126-2138.
343. Whytock, D. A., J. H. Lee, J. V. Michael, W. A. Payne and L. J. Stief, 1977, J. Chem. Phys., **66**, 2690-2695.
344. Whytock, D. A., J. V. Michael and W. A. Payne, 1976, Chem. Phys. Lett., **42**, 466-471.
345. Wine, P. H., N. M. Kreutter and A. R. Ravishankara, 1979, J. Phys. Chem., **83**, 3191.
346. Wine, P. H. and A. R. Ravishankara, 1982, Chem. Phys., **69**, 365-373.
347. Wolff, E. W. and R. Mulvaney, 1991, Geophys. Res. Lett., **18**, 1007-1010.
348. Worsnop, D. R., L. E. Fox, M. S. Zahniser and S. C. Wofsy, 1993, Science, **259**, 71-74.
349. Yarwood, G., J. W. Sutherland, M. A. Wickramaaratchi and R. B. Klemm, 1991, J. Phys. Chem., **95**, 8771-8775.
350. Zahniser, M. S., B. M. Berquist and F. Kaufman, 1978, Int. J. Chem. Kinet., **10**, 15-29.
351. Zahniser, M. S., J. Chang and F. Kaufman, 1977, J. Chem. Phys., **67**, 997-1003.
352. Zahniser, M. S. and C. J. Howard, 1980, J. Chem. Phys., **73**, 1620-1626.
353. Zahniser, M. S. and F. Kaufman, 1977, J. Chem. Phys., **66**, 3673-3681.
354. Zahniser, M. S., F. Kaufman and J. G. Anderson, 1974, Chem. Phys. Lett., **27**, 507-510.
355. Zahniser, M. S., F. Kaufman and J. G. Anderson, 1976, Chem. Phys. Lett., **37**, 226-231.
356. Zellner, R., G. Wagner and B. Himme, 1980, J. Phys. Chem., **84**, 3196-3198.
357. Zhang, R., J. T. Jayne and M. J. Molina, 1994, J. Phys. Chem., **98**, 867-874.
358. Zhang, R., M.-T. Leu and L. F. Keyser, 1994, J. Phys. Chem., **98**, 13,563-13,574.
359. Zhang, R., M.-T. Leu and L. F. Keyser, 1995, Geophys. Res. Lett., **22**, 1493-1496.
360. Zhang, R., P. J. Wooldridge and M. J. Molina, 1993, J. Phys. Chem., **97**, 8541-8548.
361. Zolensky, M. E., D. S. McKay and L. A. Kaczor, 1989, J. Geophys. Res., **94**, 1047-1056.